EFFECTS OF CUMULUS CLOUDS ON SOLAR RADIATION

EFFECTS OF CUMULUS CLOUDS ON SOLAR RADIATION

by

WILLIAM JAMES BLACKBURN

A RESEARCH PAPER SUBMITTED TO THE
DEPARTMENT OF GEOGRAPHY IN
PARTIAL FULFILMENT OF THE
REQUIREMENTS FOR THE
HONOURS B.A. DEGREE

McMASTER UNIVERSITY

APRIL 1978

HONOURS BACHELOR OF ARTS (1978)
(GEOGRAPHY)

McMASTER UNIVERSITY
HAMILTON, ONTARIO

TITLE: EFFECTS OF CUMULUS CLOUDS ON SOLAR RADIATION

AUTHOR: WILLIAM JAMES BLACKBURN

SUPERVISOR: DR. JOHN A. DAVIES

NUMBER OF PAGES: viii, 80

ABSTRACT:

An investigation of the effects of cumulus clouds on solar radiation was carried out during the 1977 field season at McMaster University, Hamilton. The measurement of total incoming solar radiation, direct beam radiation and the diffuse flux calculated as a residual, were used to draw inferences regarding the transmission properties of cumulus clouds, both on a daily basis and for different cloud fields, The diffuse flux, showing the greatest variability, was sub-divided into three components and each were evaluated under unobscured and obscured sun conditions. Measured values were compared with those derived for a model atmosphere.

ACKNOWLEDGEMENTS

This research project was made possible through funds provided by Dr. John A. Davies. The author wishes to express his gratitude for the continued encouragement, direction and expertise provided by Dr. Davies during the data collection period and in the finalizing of this report. Special thanks is also extended to Dr. Wayne R. Rouse for his encouragement and helpful advice towards my academic efforts.

TABLE OF CONTENTS

LIST OF FIGURES

CHAPTER I

INTRODUCTION

A. Aims of Study

There have been few attempts to monitor the effect of cumulus cloud on solar radiation. This is largely attributable to the complexities of modelling cloud behaviour since variations in multiple scattering, albedo and transmission characteristics with geometrical form must be considered. The only serious attempts in deriving cloud transmissions are those documented by Haurwitz (1945, 1946, 1948) who arrived at values for three broad cloud groups: "low", "middle" and "high" at the Blue Hill Observatory. All data were collected under overcast skies. Although Haurwitz considered a number of cloud types, he failed to collect any data on cumulus clouds. One can only infer than cumulus clouds transmit solar radiation in a similar way to other "low clouds". Consequently, the data available on cumulus cloud transmission have remained scarce; the only recent advance being the work of Robinson (1977) who dealt with isolated cubic cumulus. Thus, the need for a study to derive a set of reliable transmission values for solar radiation through cumulus is warranted; and this is the primary aim of this analysis. Data collected from field evidence will illustrate the effects of both individual cumulus clouds and different cloud fields on solar radiation. Subsequent aims will include an examination of total solar radiation (direct beam and diffuse flux) as clouds obscure the sun and

the comparison of incident solar radiation under cumulus conditions with theoretical values of a cloudless aerosol-free atmosphere.

B. Description of Site and Data Collection

Data collection was restricted to days of cumulus cloud cover; cumulus being the dominant summer cloud type. Measurements for the study were made on July 8, 9, 13 and August 18, 1977 at McMaster University. The effects of both isolated clouds and different cloud fields could be evaluated from these. Data collection on July 13 was supplemented in part, by photographs tracing the development of cumulus. Typically, clouds began forming in the late morning, often dissipating by late afternoon.

Sensors were mounted on the roof of the Burke Science building at the university. Industrial pollution from local factories is a contributing factor in determining the particulate matter in the atmosphere over the measurement site. While the primary aim of this analysis is external to the consideration of aerosols, attenuation by atmospheric dust will necessarily be presented when comparing cloudless sky model calculations in an aerosol-free atmosphere with cumulus cloud cover measurements. Buffalo radiosonde data were extracted from 1200 GMT ascents providing information on changes in pressure, temperature and dewpoint depression with height. Surface weather observations were recorded at Mount Hope Airport which is located 14.5 kilometres south of the measurement site at McMaster. Figure 1 shows the proximity of the Surface Weather Record station and the Upper Air station at Buffalo to the McMaster site. The value of on-site cloud observations has been discussed by Davies, Schertzer, and Nunez (1975), thus cloud observations were taken during the measurement

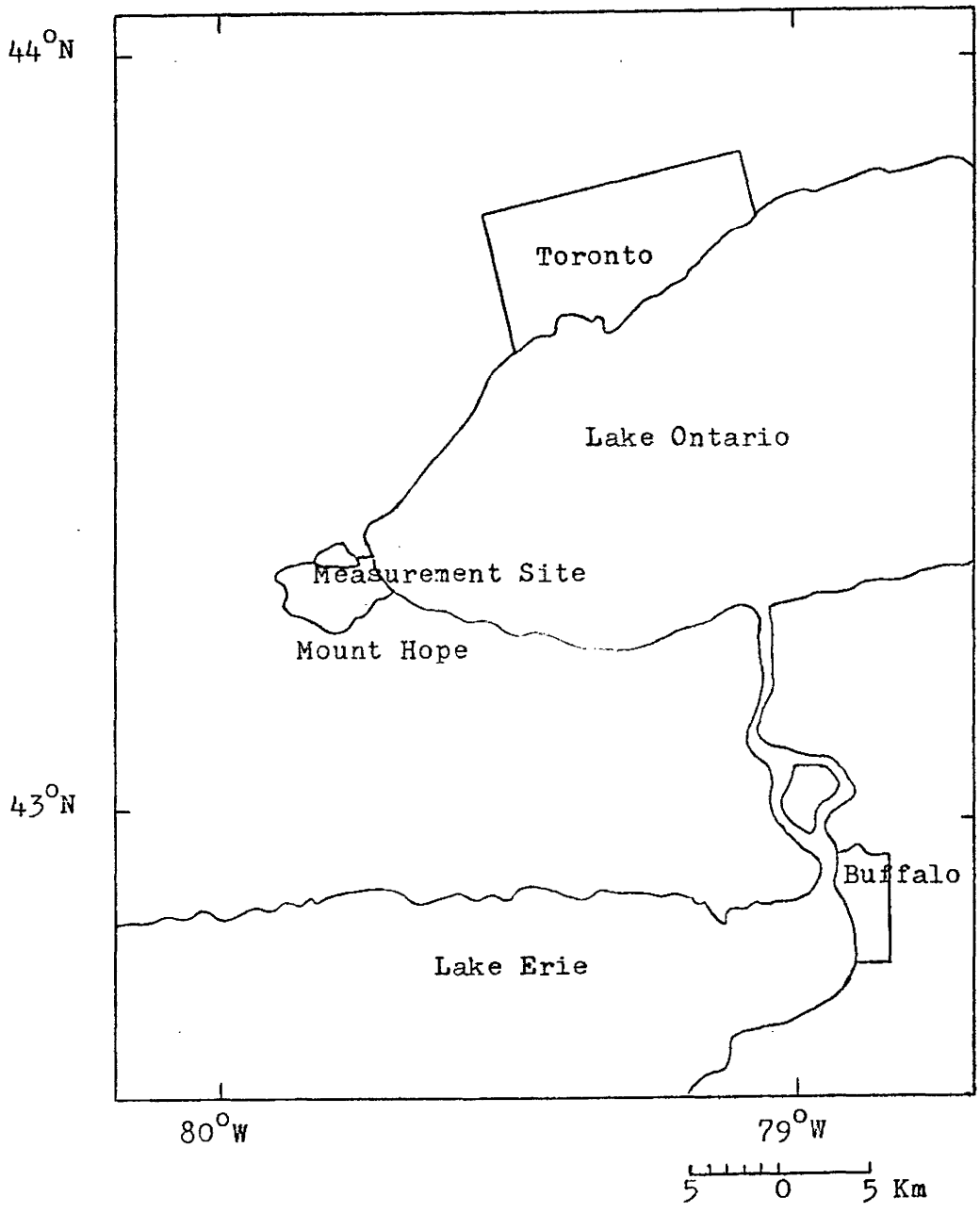

FIGURE 1: Region surrounding the measurement site at McMaster, including the location of the surface weather records site (Mount Hope) and the site of the upper air station (Buffalo).

periods at McMaster. Since cloud observation is arbitrary, a maximum difference of two-tenths cloud cover was allowed between Mount Hope and the on-site observations. Most of the values obtained for cloud fields fell within this range. On selected days, cumulus clouds were photographed to demonstrate their sequential development and dynamic nature.

CHAPTER II

INSTRUMENTATION AND METHODOLOGY

A. Measurements

Measurement of the direct beam solar radiation I was made with an Eppley Normal Incidence Pyrheliometer (NIP) while the total incoming solar radiation (direct beam and diffuse flux) $K\downarrow$ was measured with a Precision Eppley Pyranometer. Since

$$K\downarrow = I\cos Z + D \tag{1}$$

where cosZ is the cosine of the solar zenith angle and D is the flux of diffuse from the sky and cloud; diffuse radiation was obtained as a residual.

B. Experimental Measurement Period

On June 3, 8, 9, and 10 sensor signals were recorded on a two-channel strip chart recorder (Honeywell, Model 194). The chart, running at a speed of one inch per two minutes, continuously recorded both the total incoming solar radiation and the direct beam radiation. Passage of clouds was detected as a series of maxima and minima in the radiation trace. These data were discarded because of the lack of complementary atmospheric and cloud observations and due to problems in reading values

accurately from the chart.

C. Revised Data Collection Method

Following the experimental period, the radiation fluxes were recorded on a Solartron data logger. Sensor signals were recorded on magnetic tape. Signals were scanned once every ten seconds. The new procedure did not provide an immediate visual record but it did provide data to three significant decimal places. When the magnetic tape was processed by computer, maxima and minima were extracted from the initial output, corrected and calibrated. These data were ultimately used in the calculation of transmission values.

One logger channel was shorted to obtain a measuring system zero. Each sensor signal was corrected by the amount that the shorted channel deviated from zero. The entire procedure is outlined in Figure 2.

D. Sensors

(i) Normal Incidence Pyrheliometer

The Eppley Normal Incidence Pyrheliometer was used in the measurement of direct beam solar radiation. The instrument consisted of two parts: (a) an Eppley Solar Tracker, which was electrically driven and geared to solar time, designed to accomodate the normal incidence pyrheliometer, and (b) the NIP itself for total (or spectral) measurements of solar radiation at normal incidence.

The sensor was set up in a north-south direction. This setting allowed the axis of rotation of the earth and the tracker to be in the

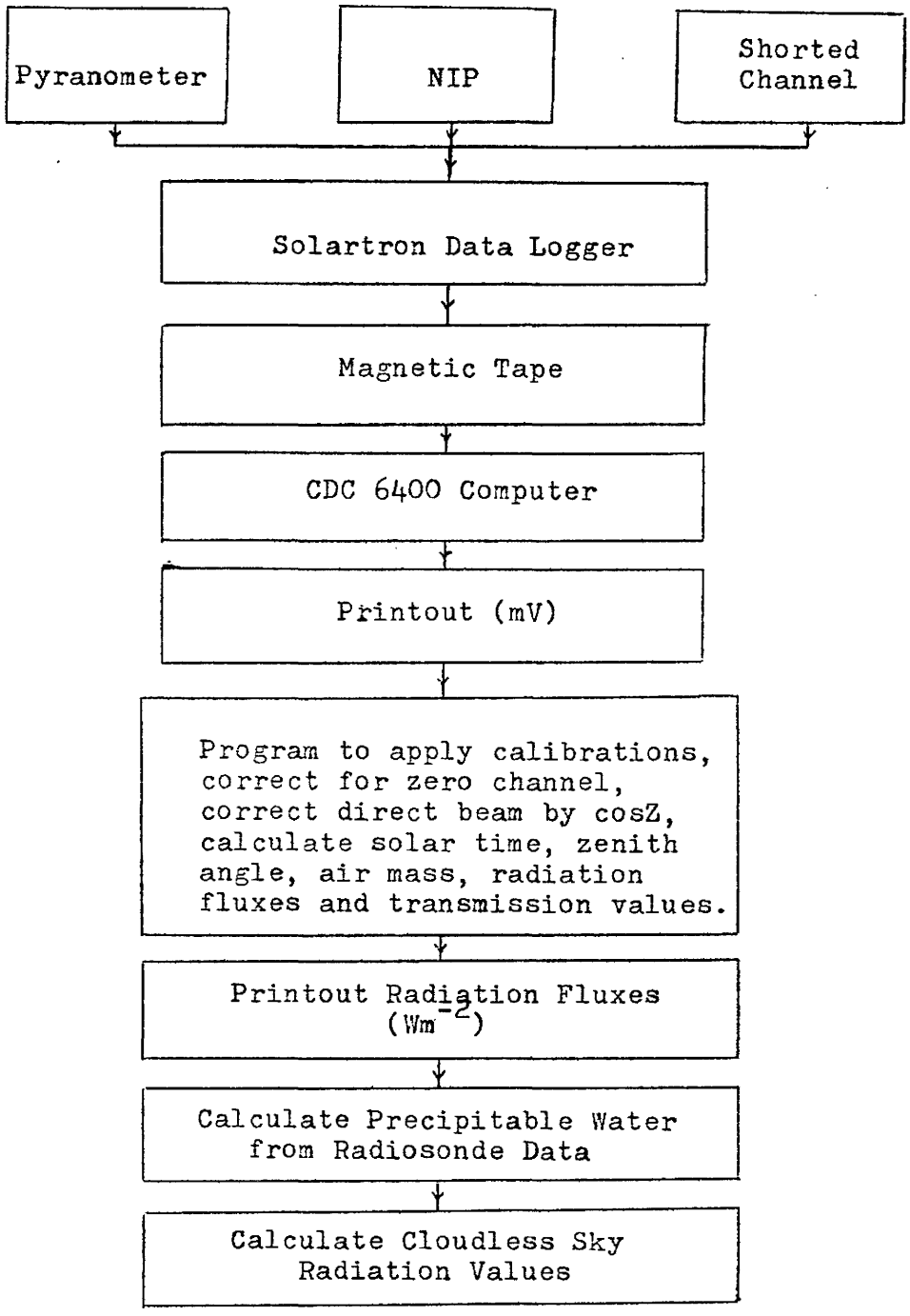

FIGURE 2: Data collection procedure and calculation of cloudless sky solar radiation.

same plane. The geographical north-south meridian was determined by knowing the location of a distant antenna on the Niagara Escarpment and the drive end of the tracker was set up such that it was facing south, aligned to this reference point. The instrument was then set for latitude, solar declination and time. The latitude was a fixed parameter, but it was necessary to reset the solar declination periodically. Once the pyrheliometer had been mounted and the leads connected to the Solartron recorder, the sensor was aimed directly at the sun, using a light spot sight. For accurate measurements, the light spot was not allowed to drift further than two diameters from the target.

The thermopile used in the NIP is of wire-wound construction with a 3/8 inch square receiver, Eppley nomenclature E type. It is mounted at the base of a brass tube. The aperture (standard field of view established by the W.M.O.) bears a ratio to it's length of 1 to 10, subtending an angle of 5° 43' 30". The inside of this tube is blackened and suitably diaphragmed. The tube is filled with dry air at atmospheric pressure and sealed at the viewing end by a removable insert carrying a crystal quartz window 1 mm thick.

The thermoelectric effect is produced by plating the constantan wire with copper, thus producing a copper-constantan junction. A mylar receiver is then cemented to a set of hot junctions and painted with 3M black.

(ii) Eppley Precision Spectral Pyranometer

The Precision Eppley Pyranometer was used to measure total incoming solar radiation. It comprises a circular multi-junction Eppley

thermopile of the wire-wound type. It's receiver is coated with Parson's black lacquer (nonwave-length-selective absorption). This instrument has a pair of removable precision ground and polished hemispheres of Schott optical glass (the inner of clear WG7 glass, the outer of WG7 glass). The WG7 glass is transparent from a wave-length of about 285 to 2800 mμ.

CHAPTER III

THE NATURE OF CUMULUS CLOUD

A. Cloud Photography at the Measurement Site

Throughout the summer field season cumulus were noted to commence forming at approximately 1400 GMT, often dissipating by late afternoon. July 13, 1977 was chosen as a day on which the formation of cumulus cloud could be monitored by photographs. Atmospheric conditions were ideal with intense solar radiation, minimal wind velocity and initially clear skies (i.e. no other cloud nor haze were visible). Photographs were taken from the roof of the Burke Science building from a fixed point, each photograph covering as close as possible the same area of the sky. Considerable changes in the spatial distribution of the clouds was observed over time as single isolated cumulii formed larger consolidated groups. As the clouds developed vertically, a substantial decrease in the transmission of solar radiation was apparent. The photographs presented here serve two roles: to demonstrate the development stages of cumulus cloud and to supplement the transmission data for July 13. A visual rate of development is apparent in the photographs, since they were taken at nearly constant intervals, with the average time between photos being twenty minutes. Photos were taken over the period 1450 GMT to 1810 GMT.

Six photos have been selected for text representation corresponding to the following GMT times (the cloud field appearing in

parentheses): 1450 (1/10), 1550 (2/10), 1605 (3/10), 1635 (4/10), 1650 (6/10), and 1740 (7/10).

(a) Figure 3 (1450 GMT): Small isolated cumulus were forming with the typical flat base corresponding to the condensation level of the atmosphere. The lateral extent of the clouds was greater than the vertical development.

(b) Figure 4 (1550 GMT): Cloud size and number were increasing, but vertical development remained limited.

(c) Figure 5 (1605 GMT): An extensive increase in cloud number had occurred since the previous photo. Lateral development still dominated as the clouds took on a more characteristic form. The condensation level was recognized more easily.

(d) Figure 6 (1635 GMT): Lateral development was now extensive, but vertical development was limited. An increase in absolute cloud size was apparent as well as the clustering of medium-sized clouds.

(e) Figure 7 (1650 GMT): Clouds reached greater absolute size as vertical development began to play a more dominant role.

(f) Figure 8 (1740 GMT): The extent of vertical development dramatically increased as the clouds become more massive in appearance. It became increasingly difficult to distinguish between individual clouds as clustering of clouds occured and as wind speed increased slightly.

Following the photographic period vertical development increased and ground observations became difficult since very packed continuous clusters of varying scale cumulii formed. Mount Hope Surface Weather Records indicated a continuous decrease in cloud field to 2/10 cumulus at 0000 GMT. These photographs as a group serve to illustrate the dynamic nature of cumulus over time and space, the critical factor being the vertical component.

FIGURE 3: (1450 GMT, 1/10 cloud field)

FIGURE 4: (1550 GMT, 2/10 cloud field)

FIGURE 5: (1605 GMT, 3/10 cloud field)

FIGURE 6: (1635 GMT, 4/10 cloud field)

FIGURE 7: (1650 GMT, 6/10 cloud field)

FIGURE 8: (1740 GMT, 7/10 cloud field)

B. Modelling Complications

Deterministic models in climatology provide a method of simulating atmospheric processes. These models are either empirically or physically based. The latter are more generally applicable since they consider the actual physical processes occuring in the earth-atmosphere system. Studies including those of Houghton (1954), Monteith (1962), Idso (1969) and Hay (1971) have employed this approach. Complexities arise when aerosols are considered, since amounts, vertical distribution and physical properties are poorly known. Clouds pose greater problems because:

(a) they are dynamic

(b) they occur at multi-levels in the atmosphere, often with several cloud types at the same level

(c) they attenuate the solar beam; a result of their absorbing and scattering capabilities

(d) cloud reflectivity is highly variable depending on cloud thickness and type

(e) multiple reflection occurs between clouds, and between cloud base and the earth's surface

The composite result is that quantitative assessment of cloud behaviour is extremely difficult.

CHAPTER IV

TRANSMISSION OF SOLAR RADIATION THROUGH CUMULUS

A. The Early Work of Haurwitz

Haurwitz (1945, 1946, 1948) focused on the relationships between solar irradiance, cloud density and cloud type. His observations and records for study were obtained at the Blue Hill Meteorological Observatory of Harvard University during two long-term periods: 1933-1943 and 1938-1945. Haurwitz (1945) was mainly concerned with solar irradiance and cloud density to derive formulae for average meteorological conditions. He chose to express K↓ as a function of air mass:

$$K\downarrow = \frac{a}{m} e^{-bm} \qquad (2)$$

where: m = air mass

e = base of natural logarithms

a, b = constants derived from least squares linear regression

Employing this relationship Haurwitz (1946, 1948) examined the relationship between incoming solar radiation and cloud type. This study was confined to days when the sky was completely overcast (i.e. 10/10 cloud field) and excluded cirrocumulus, cumulus and cumulonimbus due to lack of data.

Under cloudless skies Haurwitz (1945) related irradiance to

optical air mass by

$$K\downarrow_o = (94.4/m)\ e^{-0.059m} \tag{3}$$

The ratio of K↓ with overcast skies to that of clear skies can be written as

$$K\downarrow/K\downarrow_o = (a/94.4)\ e^{-(b-0.959)m} \tag{4}$$

Haurwitz concluded that all clouds could be grouped into three generic classes with associated transmission capabilities:

Cloud Group	Reduction in K↓	% K↓ Transmitted
high	20	80
middle	50 - 60	40 - 50
low	65 - 80	20 - 35

It is noteworthy that these values are based on observations from one station in the middle latitudes and that the transparency of various cloud types may be different under different climatic conditions. However, this is virtually the only study that may be referenced as a guideline against which results obtained in the present analysis may be compared. Although Haurwitz excluded cumulus cloud from his analysis, cumulus does belong to the "low" cloud group. This connotation will be employed for the duration of this analysis and it will be hypothesized that cumulus cloud transmit 20-35% of the total solar radiation incident upon them.

B. Calculation of Transmission Values

In order to calculate the amount of solar radiation transmitted through cumulus cloud it is necessary to first obtain flux measurements of the incoming solar radiation in an atmosphere without cloud. This will allow a comparison between cloudless skies and radiation fluxes when cloudy conditions prevail. Most methods, such as the one employed by Haurwitz (1948) use ratios of the form $K\downarrow/K\downarrow_0$ where $K\downarrow$ is the incoming solar radiation in a cloudy atmosphere and $K\downarrow_0$ is the incoming solar radiation in a cloudless atmosphere. This method suffices for comparing the atmosphere under different conditions on different days, but is not suitable for this present analysis. In this study, an unobscured atmosphere will be defined as the period in which $K\downarrow$ reaching the sensor is unaltered by cloud (i.e. most of the $K\downarrow$ flux is direct beam). An obscured atmosphere will be defined as the period in which clouds obscure the sun and consequently most $K\downarrow$ reaching the earth's surface is diffuse. Therefore, the state of the atmosphere is defined by cloud position at the time of measurement. If $K\downarrow$ before cloud obstruction is K_{max} and $K\downarrow$ during cloud is K_{min}, then the total reduction R in incoming solar radiation as a percentage of the original flux may be expressed as:

$$R = ((K_{max} - K_{min})100\%)/K_{max} \tag{5}$$

therefore, total solar radiation transmitted T through cumulus cloud is given by:

$$T = 100\% - R \tag{6}$$

This method has been employed to determine transmission. The K_{max} and K_{min} values were initially a series of maxima and minima milivolt signals from the pyranometer which were calibrated and corrected before being used in the calculation of R. This procedure forms the basis of the frequency distributions which follow of percent K↓ transmitted.

C. Cumulus Cloud Transmission

Cloud transmittances for July 8, 9, 13 and August 18 are shown in Figures 9, 10, 11 and 12.

July 8

Measurements were made with the Solartron recording system. Cloud was dissipating following overcast on the previous three days. Cloud amount ranged between 8/10 at the beginning of the measurement period and 5/10 at the end. Haurwitz (1948) found that transmission of cumulus cloud was in the 20-35% range. Figure 9, however, shows that the highest frequency of transmittance occurs in the 70-79.9% range. These larger transmittances may be explained by the presence of stratocumulus cloud. Since the day was characterized by a dissipating overcast sky and the accuracy of ground observation is controlled by the "limited window", higher level clouds may be present above the cumulus, but are not visible, and are not recorded. In the hourly cloud observation immediately prior to the measurement period, Mt. Hope had reported 9/10 stratocumulus (and no cumulus). It is assumed that some of these clouds were still present during the early part of the measurement period. While both cumulus and stratocumulus belong to the "low cloud" group, their appearance and ultimately their behaviour

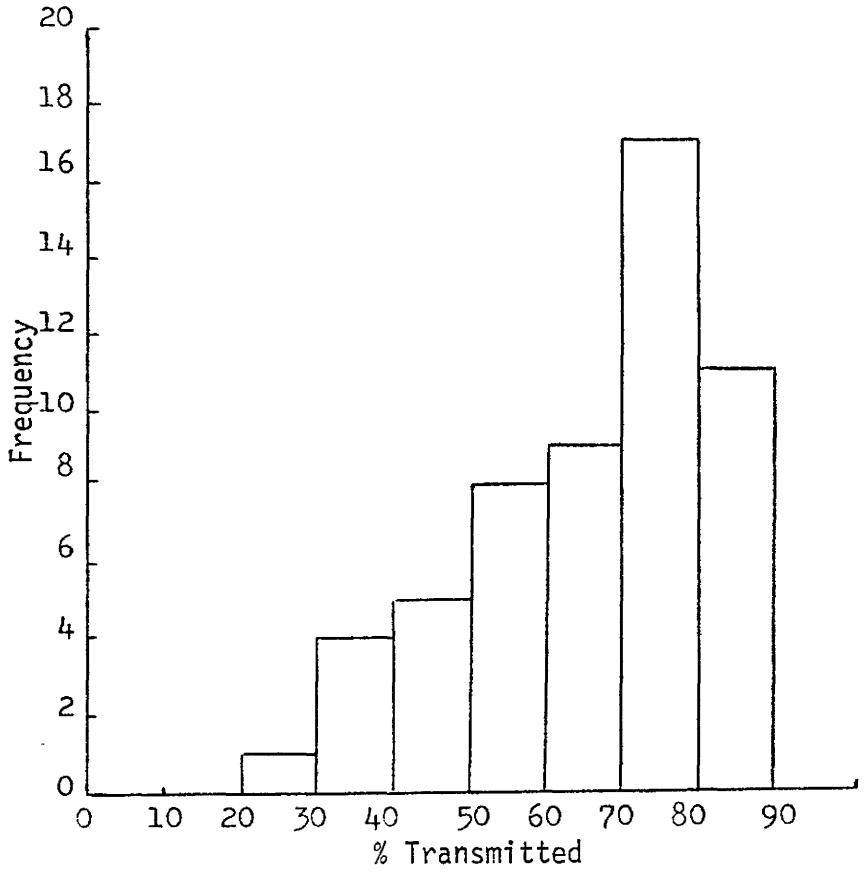

FIGURE 9: Frequency distribution of percent K↓ transmitted for July 8.

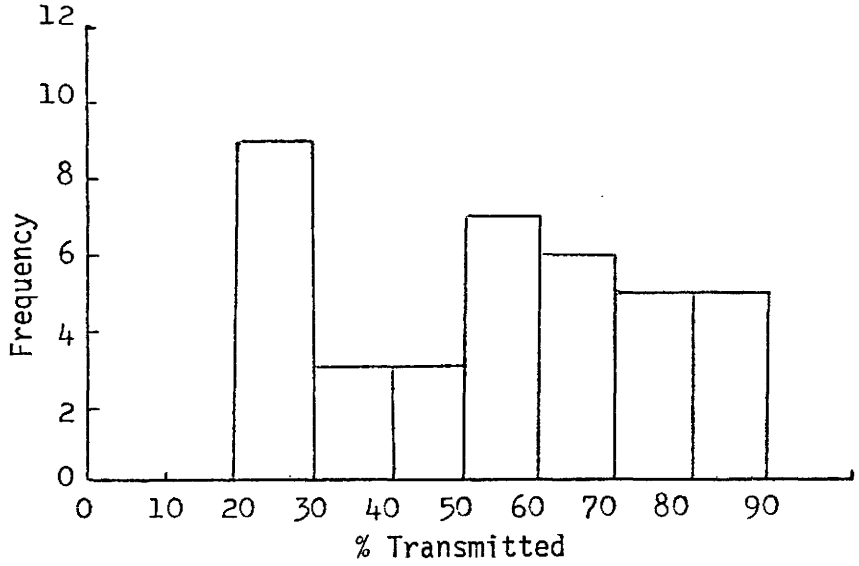

FIGURE 10: Frequency distribution of percent K↓ transmitted for July 9.

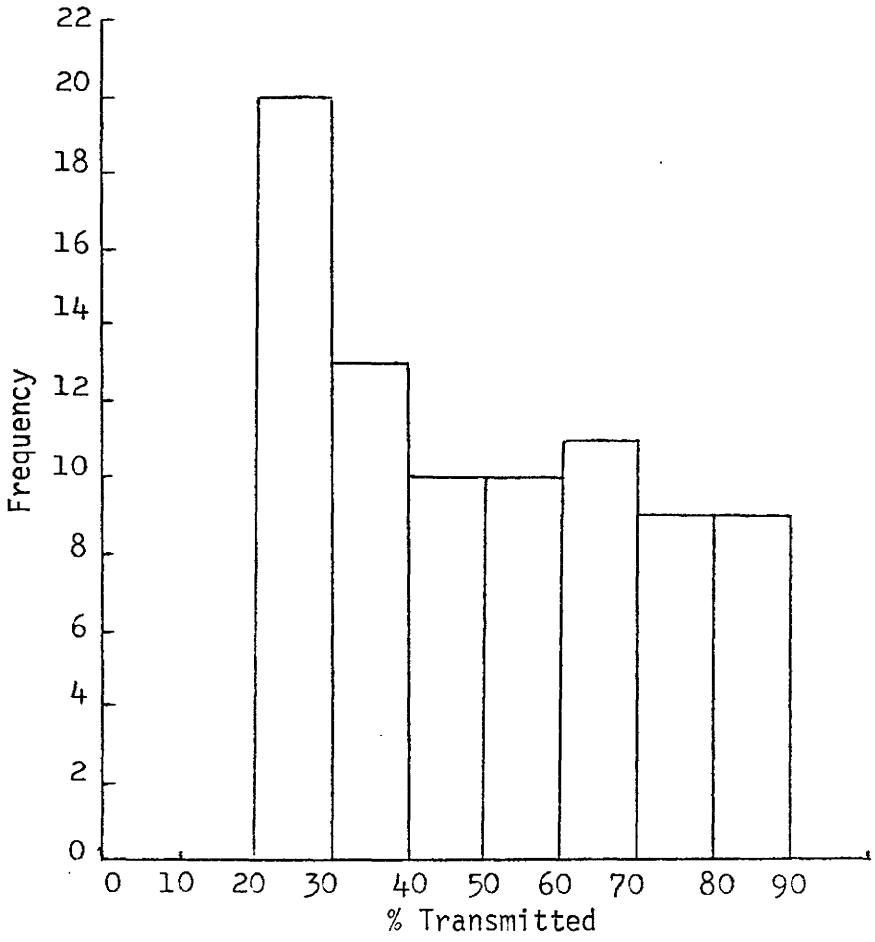

FIGURE 11: Frequency distribution of percent K↓ transmitted for July 13.

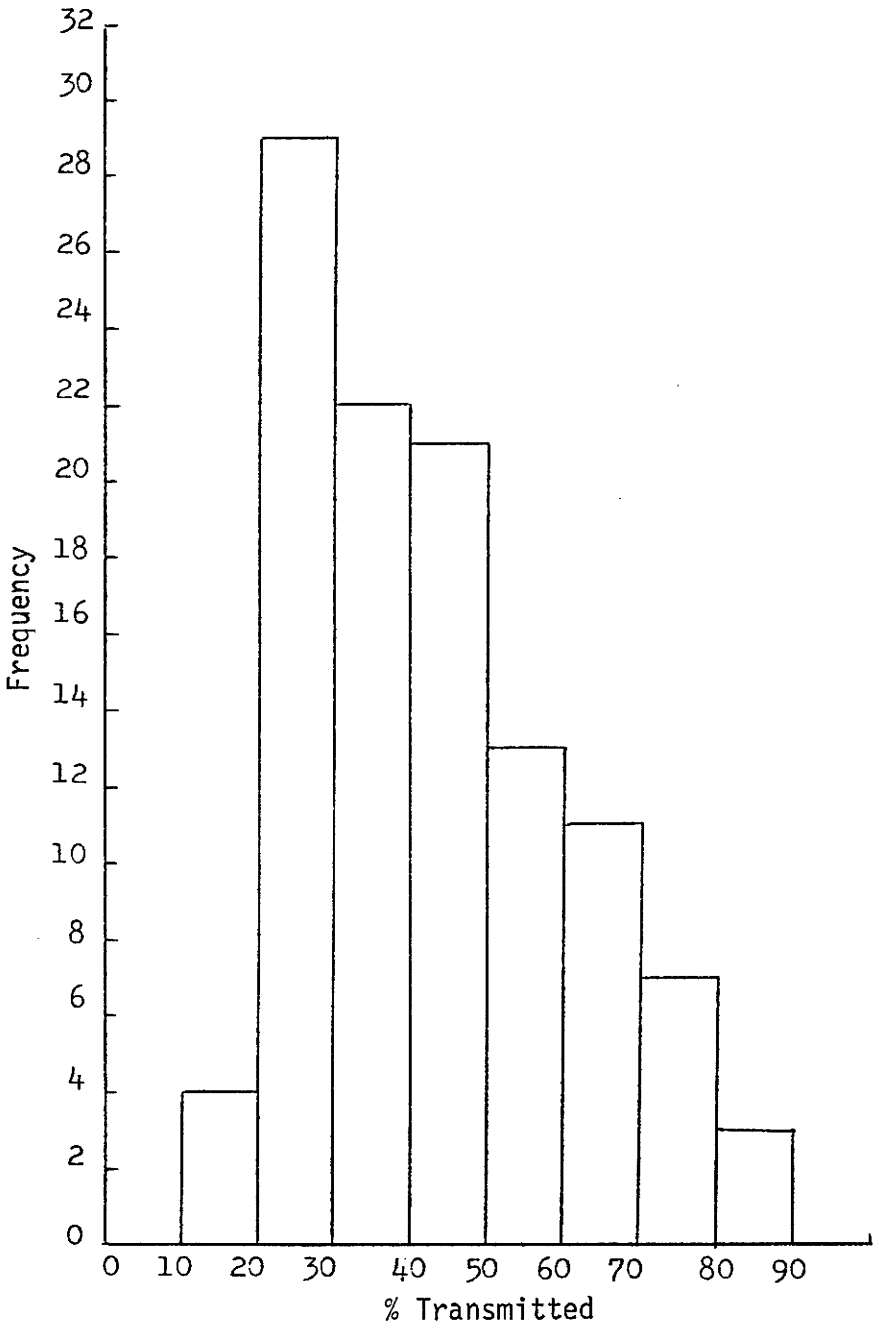

FIGURE 12: Frequency distribution of percent K↓ transmitted for August 18.

in intercepting the solar beam is different. Larger transmittance values suggest minimal cloud since they possess a relatively uniform thickness unlike cumulus where transmittance decreases with vertical development of the cloud cover. A second peak in the 90-99.9% range represents periods of time when K↓ was largely direct beam radiation when the sun was not obscured by cloud. Due to the high frequency in this interval it has not been included in the figures but is referenced in the text. This justifies the bi-modal distribution which often occurred. Wind speed during the measurement period did not exceed 5 ms^{-1} (Mt. Hope data) and hence dissipation of clouds was visible from surface observations, although the nature of cloud cover was complex and dynamic.

Two subsequent plots (Figures 13 and 14) for July 8 representing transmissions under 5/10 and 8/10 cloud cover have been constructed. The highest frequency of percent K↓ transmitted occurs in the 70-79.9% range (and 90-99.9%) ranges for 5/10 cover, and in the ranges 50-59.9, 70-79.9 (and 90-99.9%) for 8/10 cloud cover. Plots for subsequent days when fair weather cumulus conditions prevail show transmission values for all cloud fields (including those referenced here) as being substantially lower, usually peaking in the 20-29.9% transmission range as suggested by Haurwitz. Much of the doubt in the July 8 data is attributable to the poor observation conditions and the uncertainty from weather records of cloud types present.

July 9

Data collected on this day shows transmission for cloud amounts of 2/10, 3/10 and 5/10. Atmospheric conditions (i.e. wind speed, rate of cloud development) allowed individual clouds to be isolated and studied.

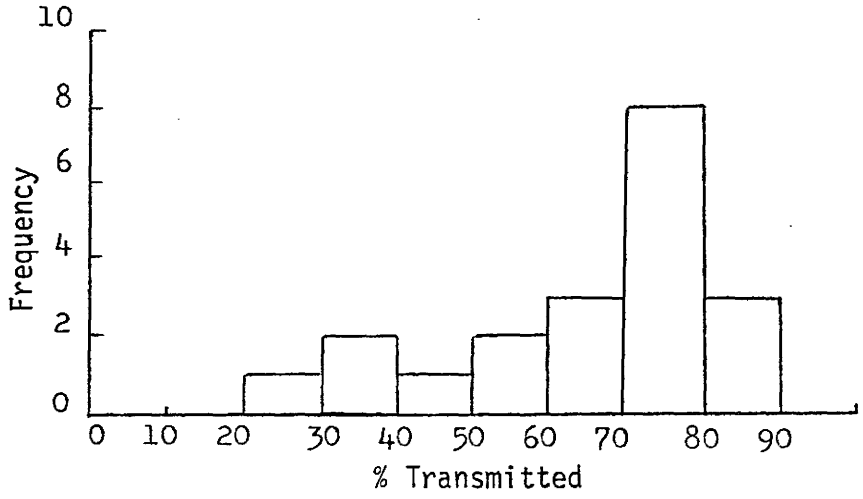

FIGURE 13: Frequency distribution of percent K↓ transmitted (5/10 cloud field) for July 8.

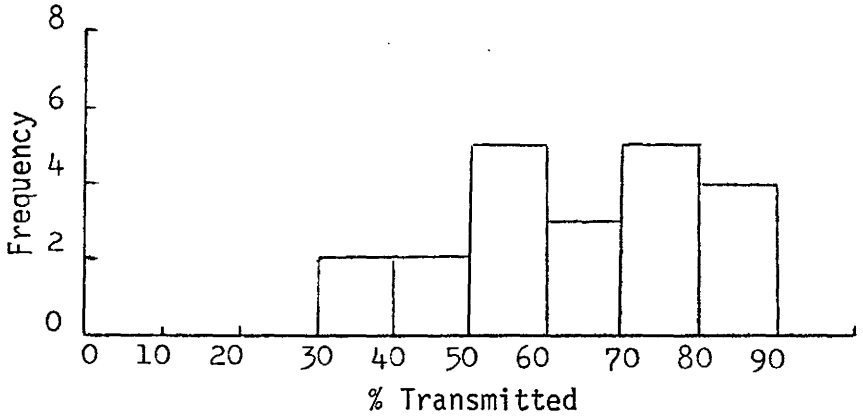

FIGURE 14: Frequency distribution of percent K↓ transmitted (8/10 cloud field) for July 8.

These data led to an analysis and quantitative justification of the phenomenon that there is a marked increase in K↓ immediately before and after a cloud obscures the sun (Monteith, 1973). Further discussion of this phenomenon appears in section G.

The daily plot shows the highest frequency of transmission in the 20-29.9% range. The plot is bi-modal, peaking again in the 50-59.9% range suggesting the presence of some stratocumulus and altostratus (Mt. Hope records these clouds between 1200 and 1300 GMT) which will allow greater transmission of radiation. The two peaks may represent distinct phases of cloud development since cloud fields of 1/10 to 3/10 persisted for several hours before 5/10 cloud fields were recorded.

All individual cloud field histograms for July 9 as shown in Figures 15, 16 and 17 exhibit a similar distribution pattern, most of them peaking in the 20-29.9% range. The only anomaly is the 3/10 cloud cover which peaks at a higher transmission level (60-69.9%) and may be attributable to the small sample size upon which the plot is based (i.e. 14 data values as opposed to 32 values for the 8/10 plot). It may be assumed with reasonable certainty that the average transmission of solar radiation through cumulus cloud is 20-29.9% which agrees with Haurwitz (1948).

July 13

Data collected on July 13 are representative of ideal cumulus cloud transmissions. On-site cloud observations agree very closely with Mt. Hope cloud observations. The wind speed was minimal, ranging from 6-8 ms^{-1} over the measurement period. The daily plot of percent K↓ transmitted exhibits the same trend as July 9, complying with assumptions

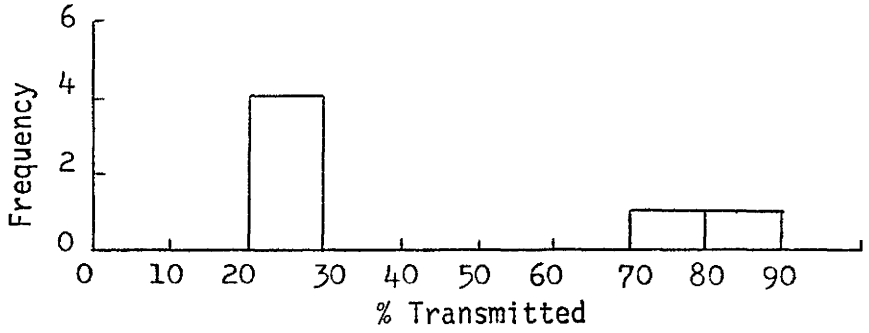

FIGURE 15: Frequency distribution of percent K↓ transmitted (2/10 cloud field) for July 9.

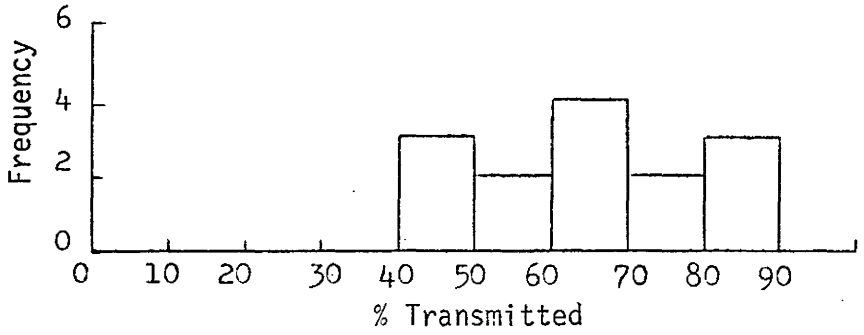

FIGURE 16: Frequency distribution of percent K↓ transmitted (3/10 cloud field) for July 9.

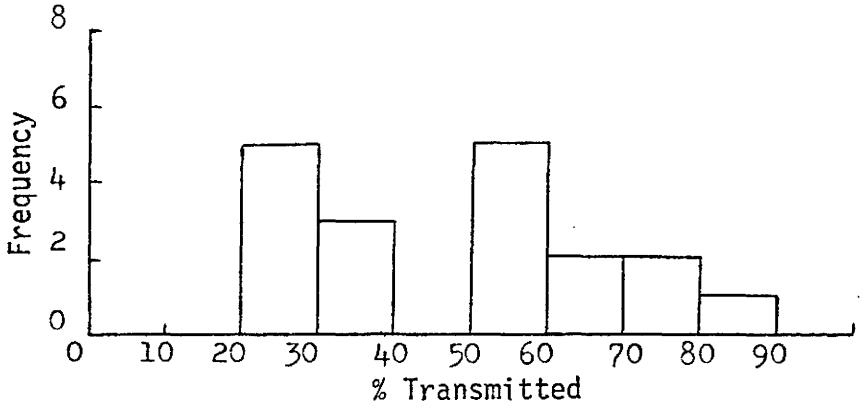

FIGURE 17: Frequency distribution of percent K↓ transmitted (5/10 cloud field) for July 9.

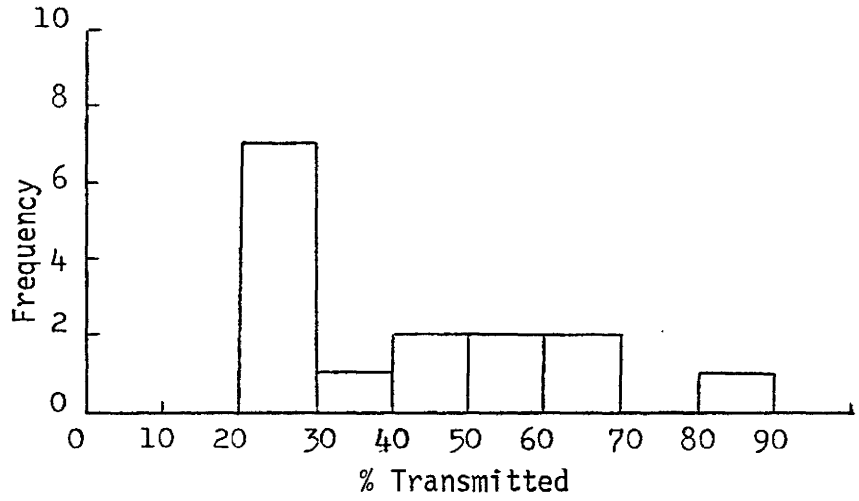

FIGURE 18: Frequency distribution of percent K↓ transmitted (6/10 cloud field) for July 13.

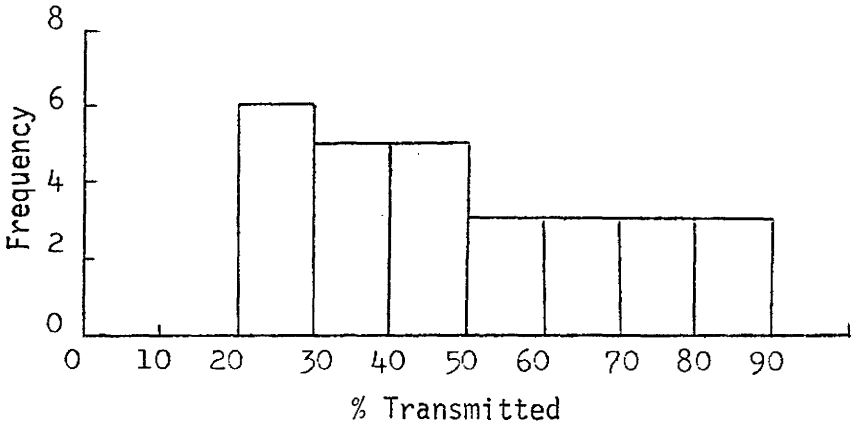

FIGURE 19: Frequency distribution of percent K↓ transmitted (7/10 cloud field) for July 13.

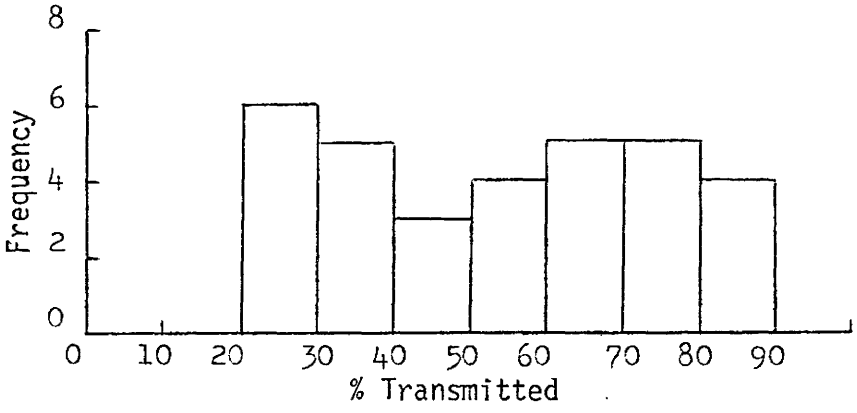

FIGURE 20: Frequency distribution of percent K↓ transmitted (8/10 cloud field) for July 13.

previously made. Maximum frequency of transmission occurs in the 20-29.9% range. As expected, a second major peak occurred in the 90-99.9% class corresponding to the clear sky intervals between clouds. Individual cloud field plots (6/10, 7/10 and 8/10) illustrated by Figures 18, 19 and 20 exhibit similar trends. The author considers these data to be the most representative collected in this study, from the point of view of illustrating the effect of single cumulus clouds on solar radiation.

August 18

Data collected on August 18 further validates the assumption that transmission of radiation under cumulus cloud is bi-modal and maximum frequency of transmission is in the 20-29.9% range. The cloud field on this day was relatively constant (6/10) over time.

D. The Diffuse Flux When the Sun is not Obscured by Cloud

Initial data analysis revealed that the diffuse radiation was subject to the greatest variation under a partly cloudy sky. Values from the raw data were selected when the direct beam radiation was at a maximum (i.e. the sun was not obscured by cloud) and the behaviour of the diffuse flux was evaluated for each of these points in time. The diffuse flux was broken up into three components: Rayleigh scattering, aerosol scattering and diffuse flux from cloud effects. Theoretical, cloudless sky, aerosol-free values were obtained from a radiation model for the direct beam, diffuse and total radiation. The diffuse component due to aerosol scattering was calculated as follows. The amount of radiation scattered from the direct beam was estimated as $(I\downarrow_o - I\downarrow_m)$ where $I\downarrow_o$ is direct beam radiation in

a cloudless, aerosol-free atmosphere and $I\downarrow_m$ is measured direct beam radiation in a partly cloudy sky when the sun is not obscured by cloud. Some portion of this appears as a component of the diffuse at the ground $D\downarrow_{as}$. Assuming the 80% of the scattered radiation is in the forward direction

$$D\downarrow_{as} = 0.8(I\downarrow_o - I\downarrow_m) \tag{7}$$

Rayleigh scattering values $D\downarrow_{rs}$ were determined from model calculations of diffuse radiation for a cloudless, aerosol-free atmosphere. The decrease in Rayleigh scattering beneath the cloud layer was accounted for in the expression

$$D\downarrow_{rs} = D\downarrow_{rs(o)}(1 - C) \tag{8}$$

where: $D\downarrow_{rs(o)}$ = Rayleigh scattering in a cloudless atmosphere

C = cloud amount in tenths

Diffuse radiation due to cloud was calculated from

$$D\downarrow_c = K\downarrow_m - I\downarrow_m - D\downarrow_{rs} - D\downarrow_{as} \tag{9}$$

where: $K\downarrow_m$ = total measured global radiation

The aerosol and cloud components of the diffuse flux were compared with values of the Unsworth and Monteith turbidity factor τ_a, which is a measure of the extinction of solar radiation by aerosol. The components of the diffuse flux were observed under different degrees of atmospheric haziness. The aerosol coefficient was obtained from

$$\tau_a = m^{-1} \ln[I\downarrow_m / I\downarrow_o] \quad (10)$$

where: m = air mass

Variations in τ_a over time for each of the four days are shown in Figures 21, 22, 23 and 24. Values of $D\downarrow_{rs}$, $D\downarrow_{as}$ and $D\downarrow_c$ normalized by the measured diffuse radiation are plotted in Figures 25-36. The largest value of τ_a (always above 0.2) occured on July 8. Values decreased throughout July 9; a response to a change in air mass. On July 13 values are relatively constant at approximately 0.15, and τ_a are low on August 18. Examination of the plots of diffuse radiation show that when diffuse radiation due to cloud is at a maximum, the magnitude of the Rayleigh scattering and aerosol scattering components is small, while the Rayleigh scattering component remains relatively constant. This is the case for August 18. On July 8, $D\downarrow_c/D$ varies between 1260 and 1285 LAT, while the effect of $D\downarrow_{rs}/D$ and $D\downarrow_{as}/D$ is minimal, having mean values of 0.2 and 0.35 respectively. Following a decrease in the cloud cover from 9/10 to 7/10, the effect of Rayleigh and aerosol scattering is increased. On July 9, τ_a peaks at 1190 LAT corresponding to a maximum (0.49) in the diffuse flux due to aerosol scattering. Diffuse radiation due to cloud is at a minimum (0.14) and Rayleigh scattering is 0.38. The data allow inferences to be drawn between the component composition of the diffuse flux and the amount of aerosol in the atmosphere at a given time. When the aerosol content of the atmosphere is low, the diffuse flux may be calculated primarily by the sum of the radiation directed toward the surface by cloud and Rayleigh scattering. If the aerosol content is high, the diffuse flux is mainly

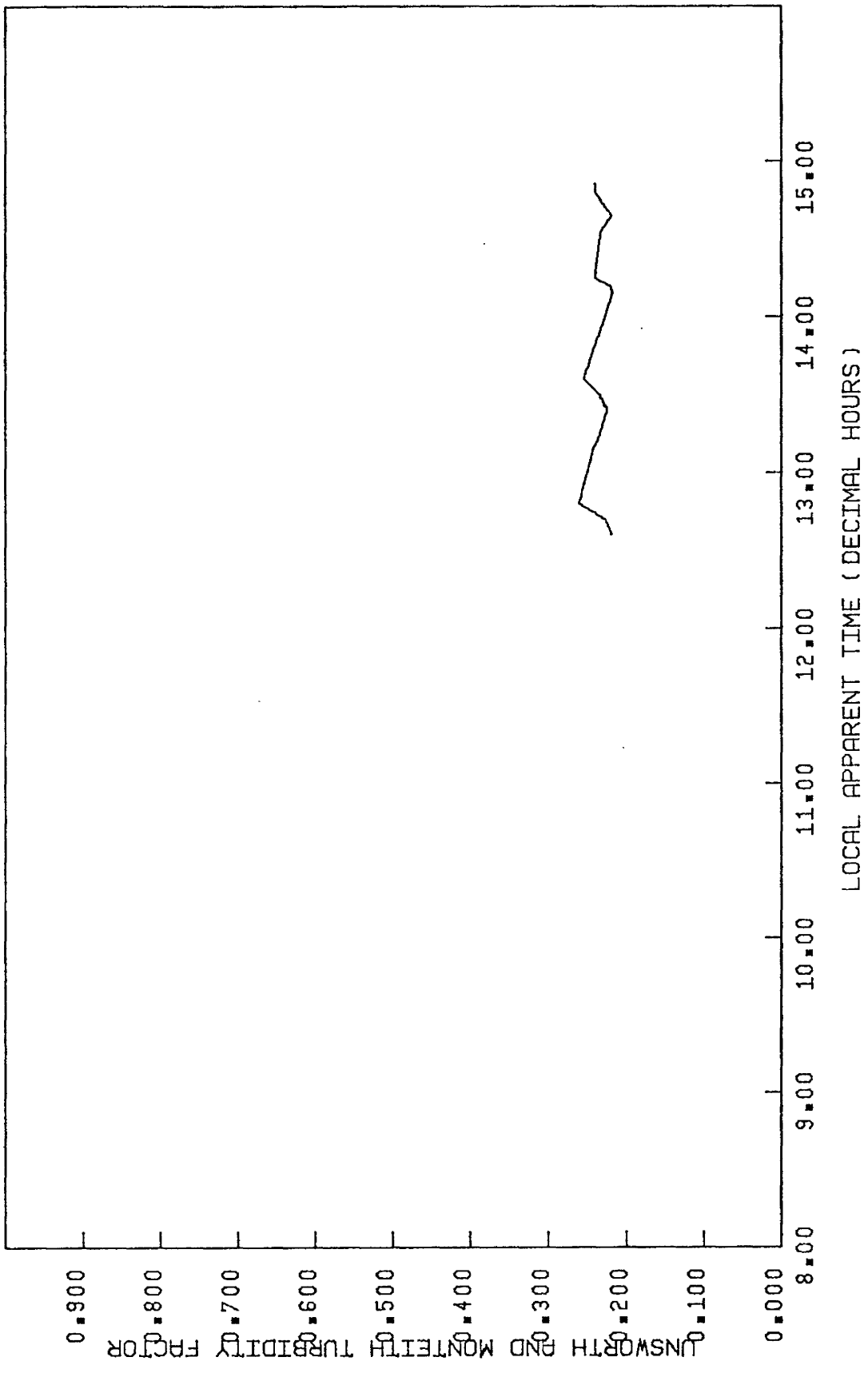

FIGURE 21: Unsworth and Monteith Turbidity Factor, July 8

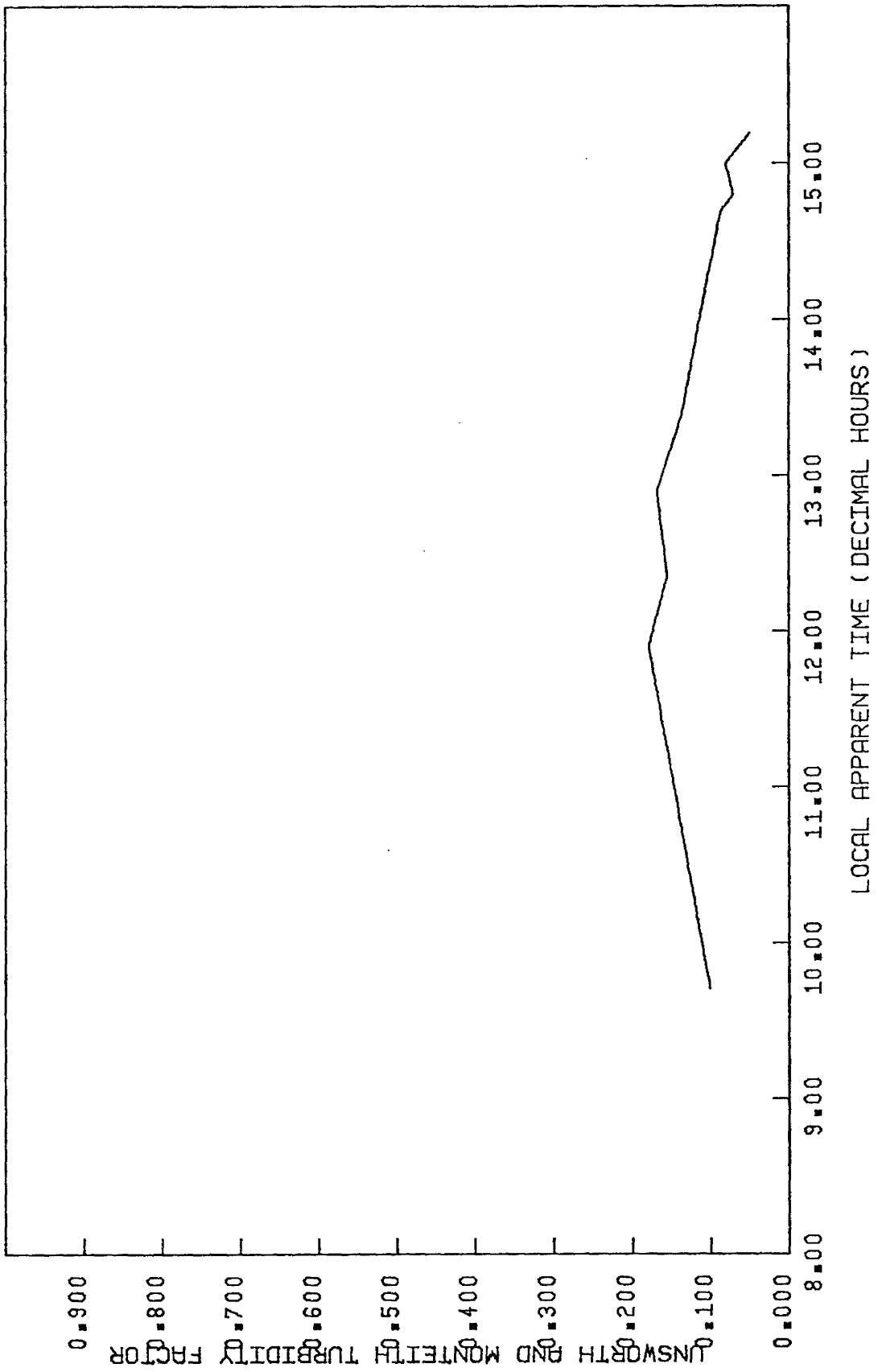

FIGURE 22: Unsworth and Monteith Turbidity Factor, July 9

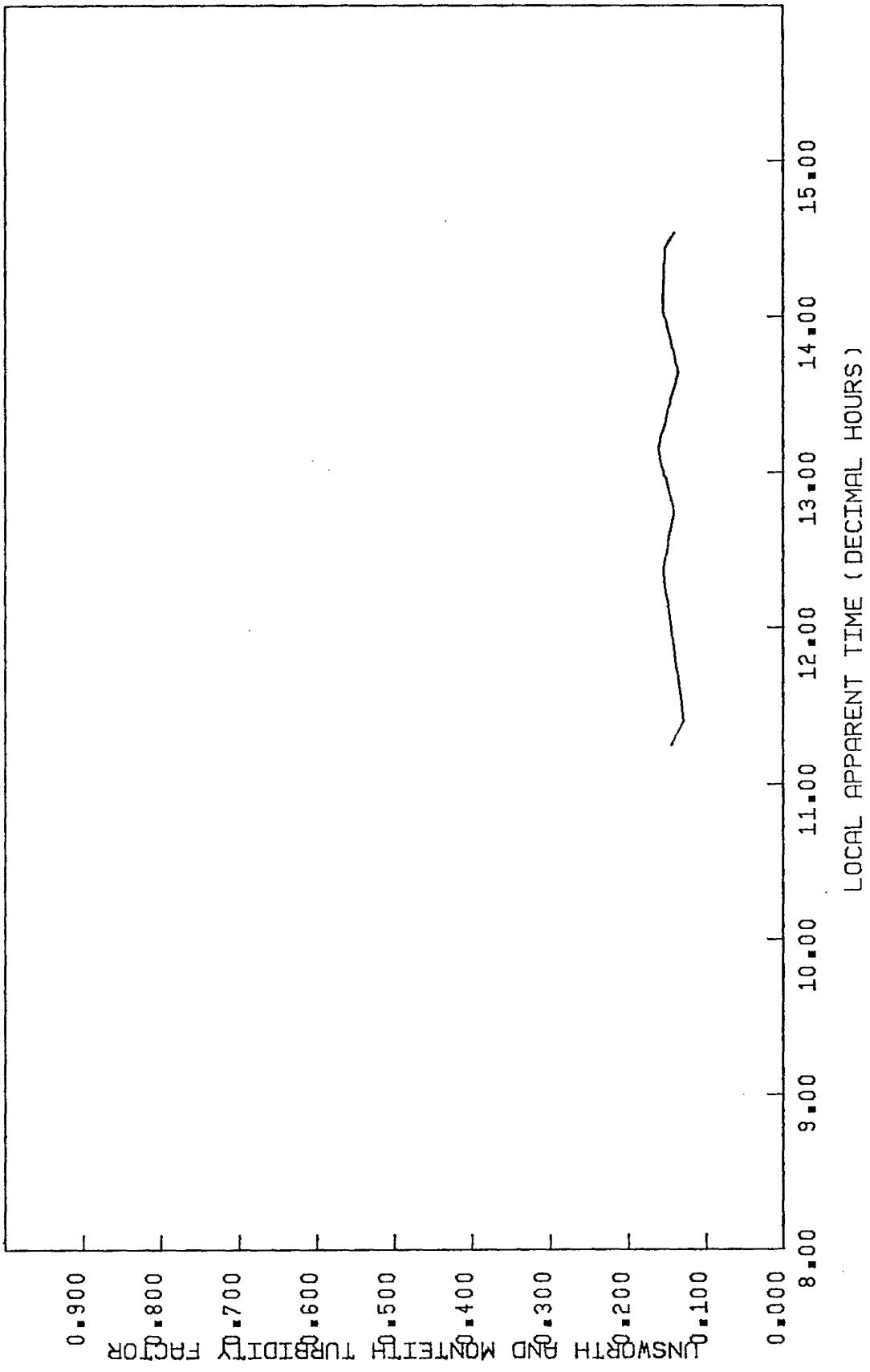

FIGURE 23: Unsworth and Monteith Turbidity Factor, July 13

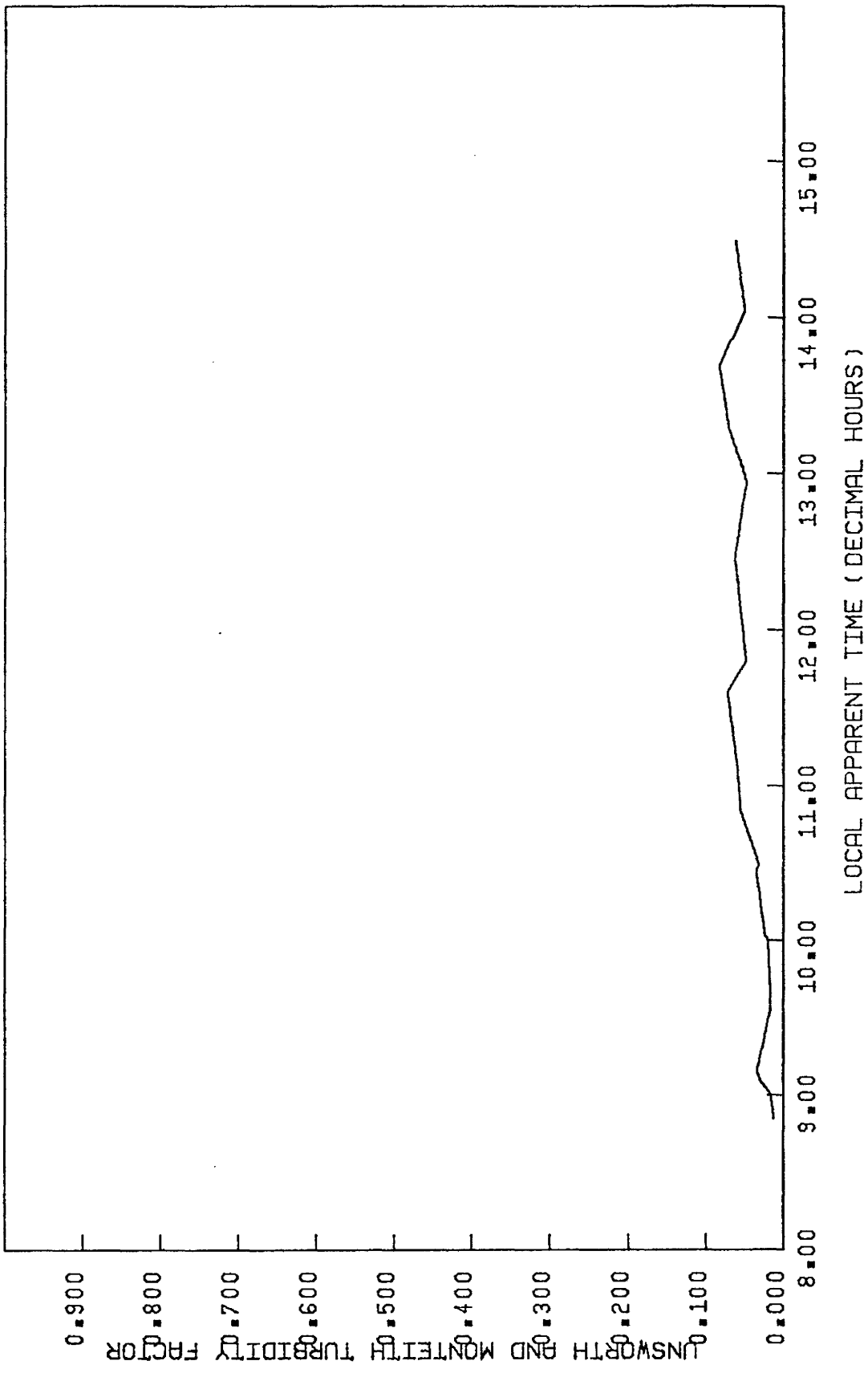

FIGURE 24: Unsworth and Monteith Turbidity Factor, August 18

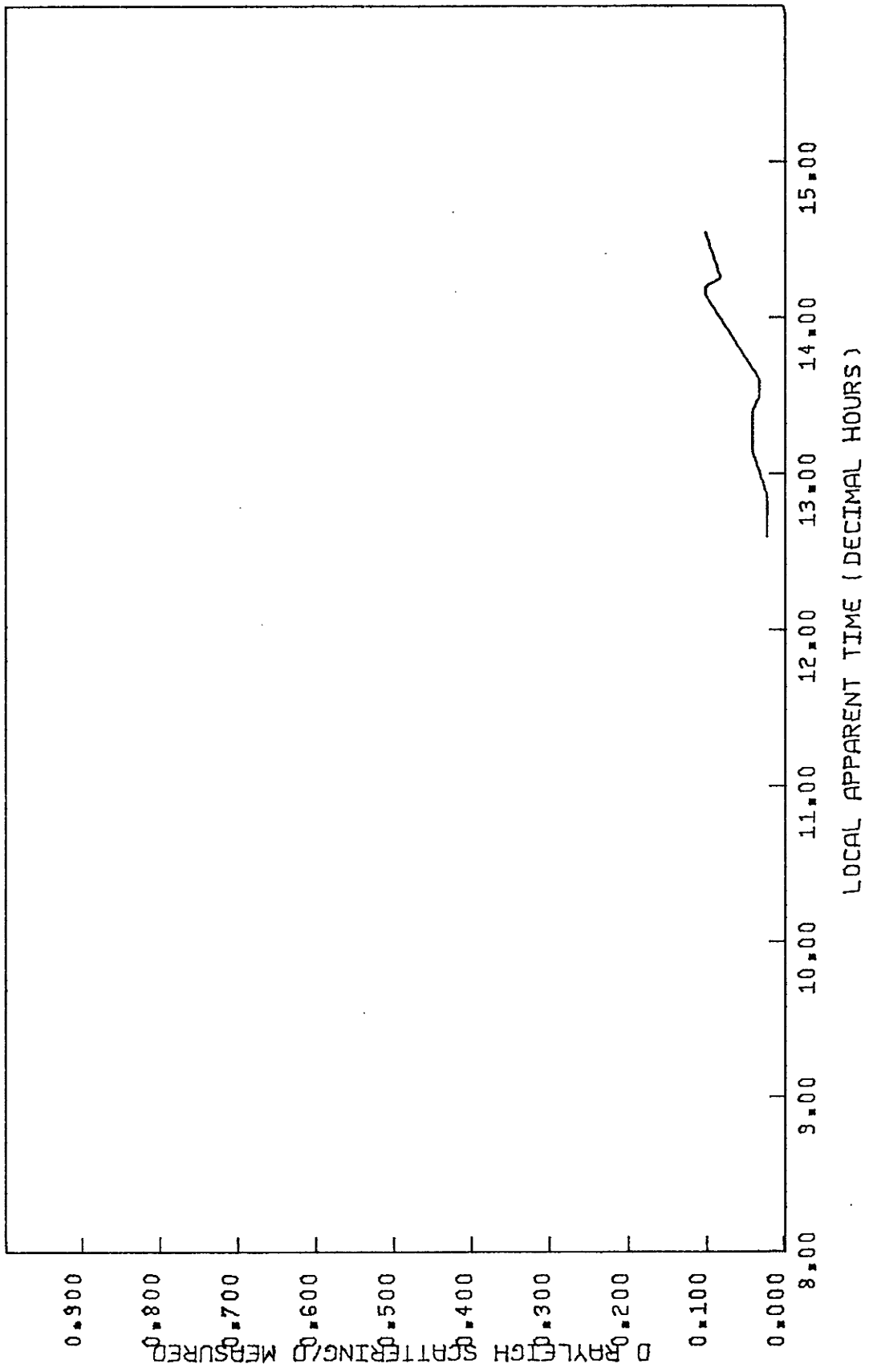

FIGURE 25: Rayleigh Scattering Component of Diffuse Radiation, July 8

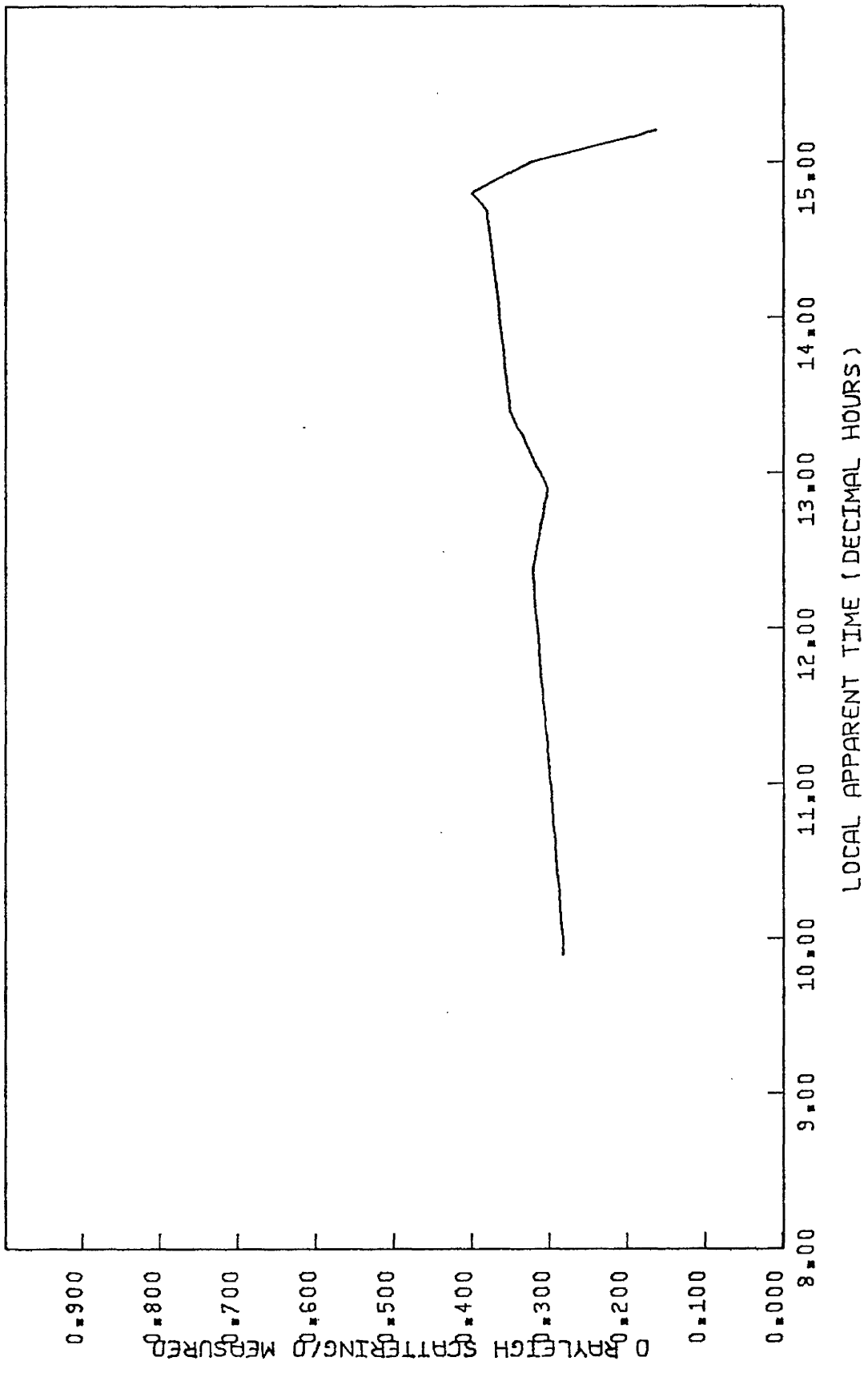

FIGURE 26: Rayleigh Scattering Component of Diffuse Radiation, July 9

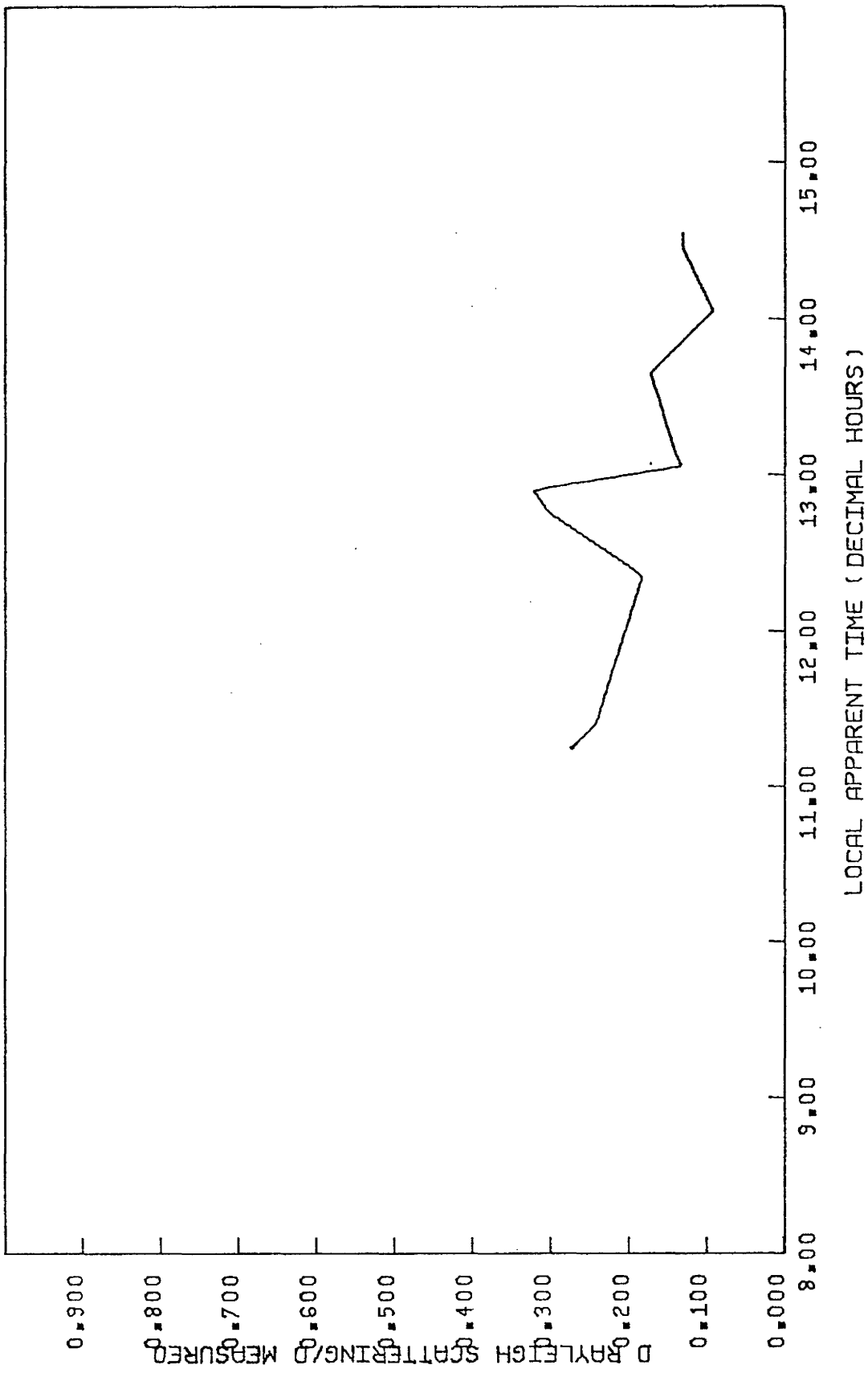

FIGURE 27: Rayleigh Scattering Component of Diffuse Radiation, July 13

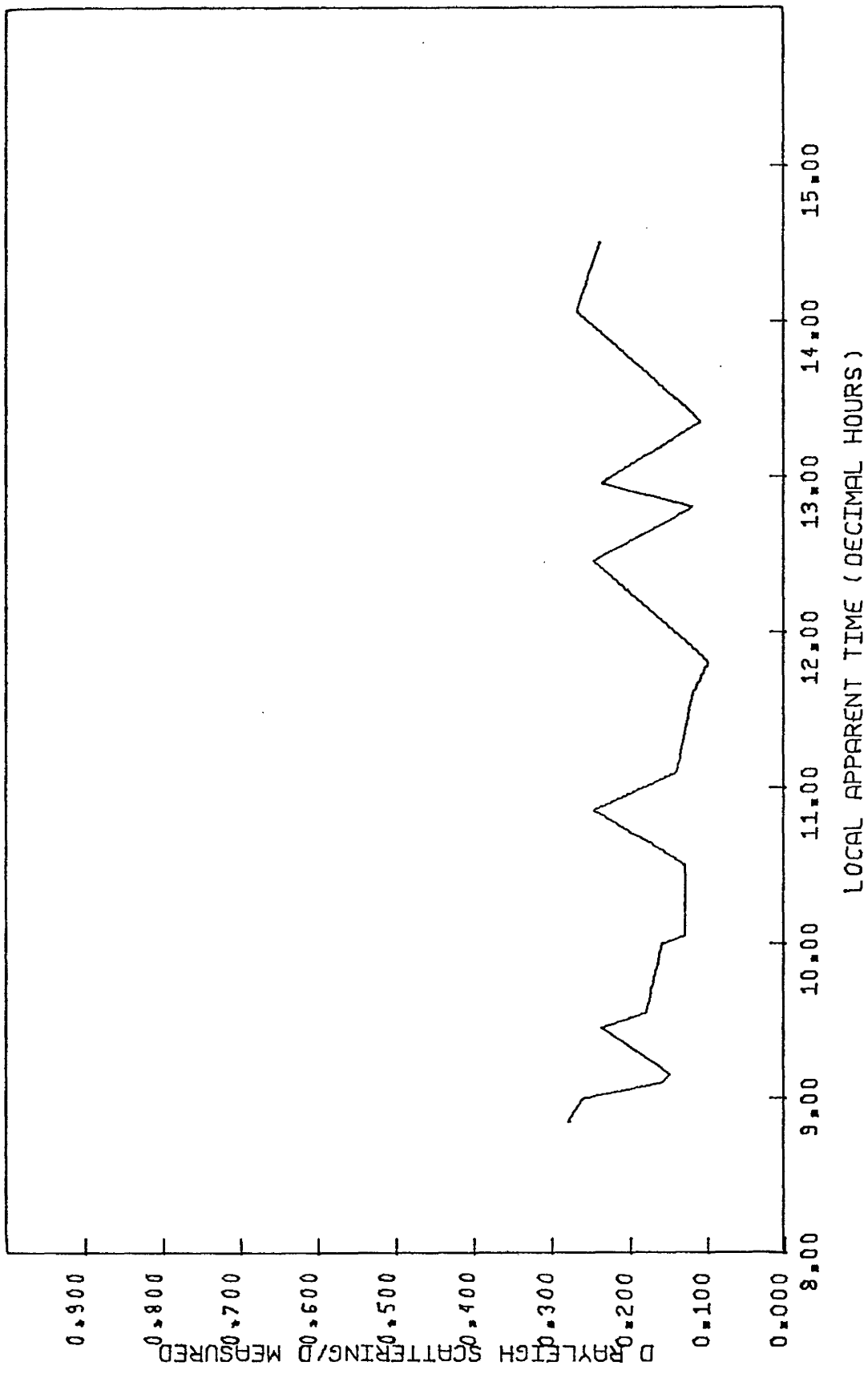

FIGURE 28: Rayleigh Scattering Component of Diffuse Radiation, August 18

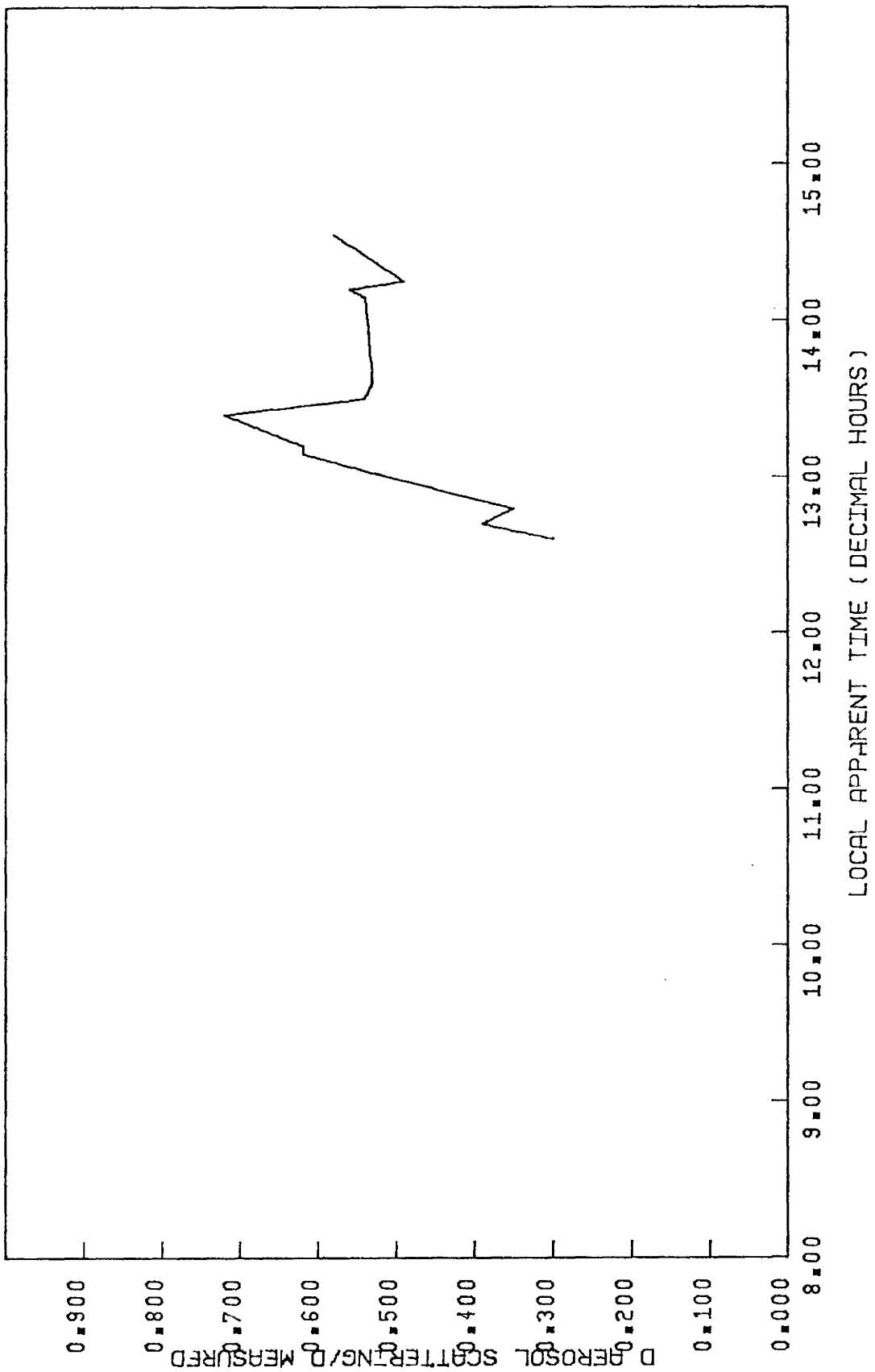

FIGURE 29: Aerosol Scattering Component of Diffuse Radiation, July 8

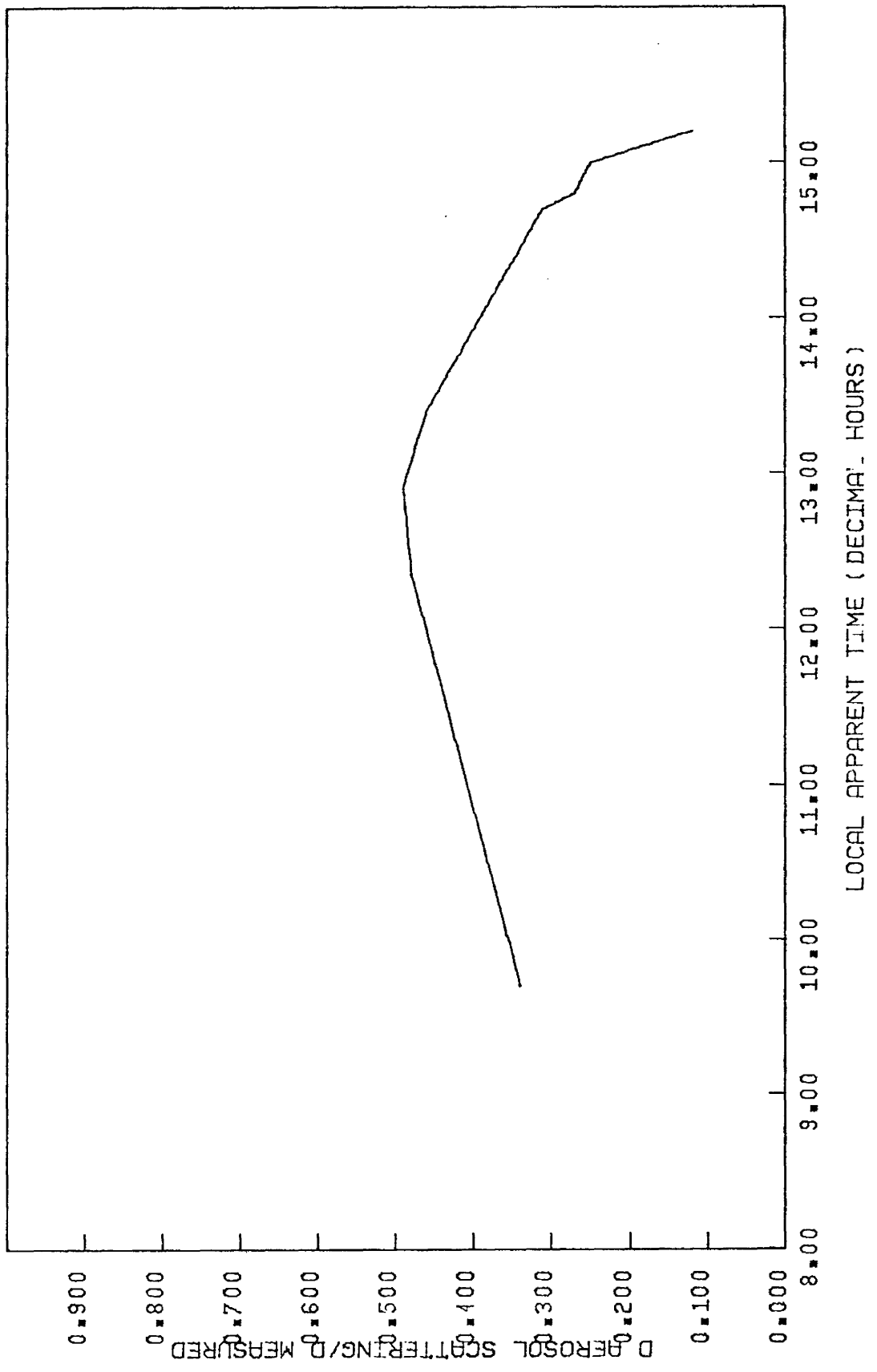

FIGURE 30: Aerosol Scattering Component of Diffuse Radiation, July 9

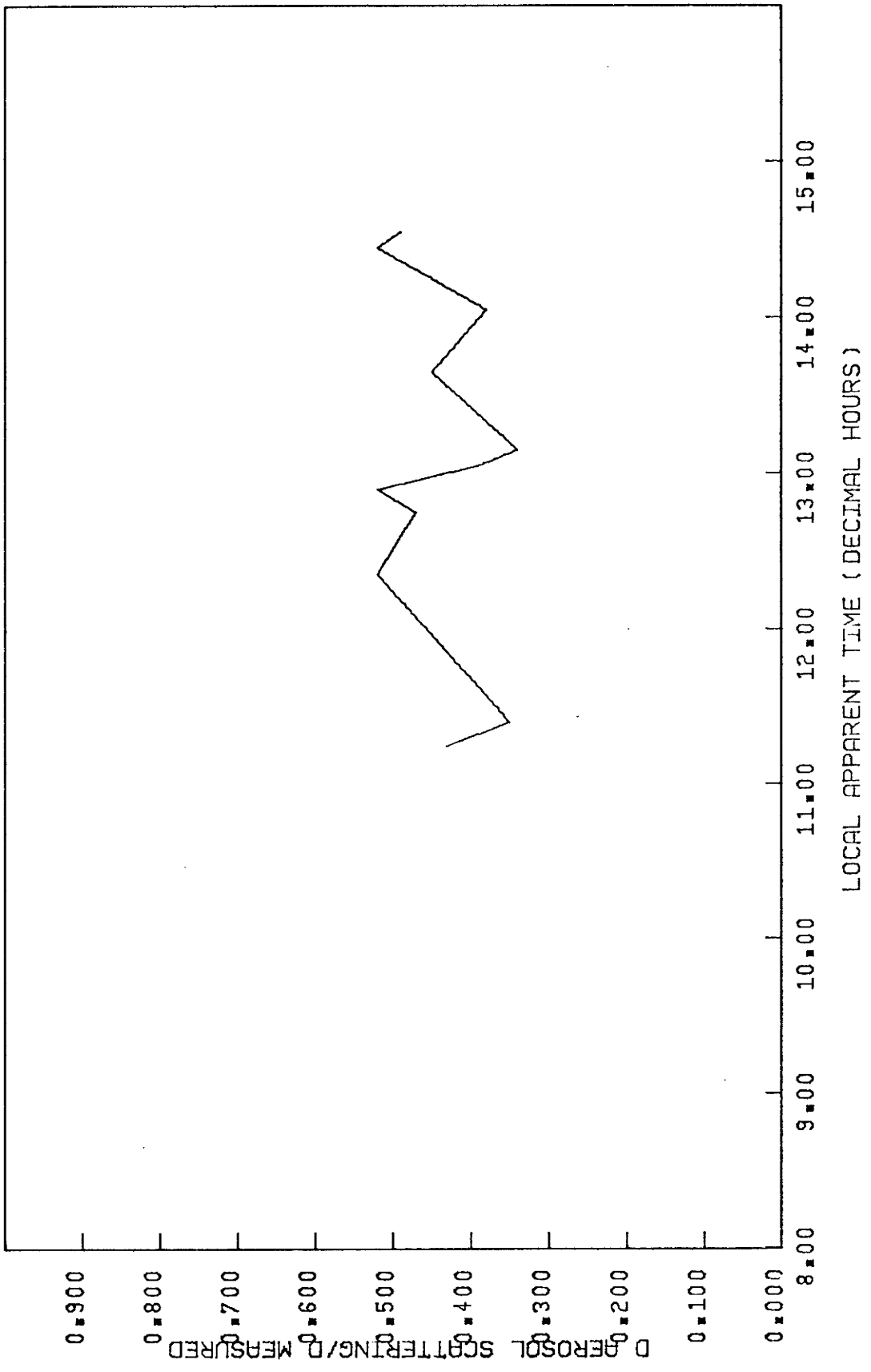

FIGURE 31: Aerosol Scattering Component of Diffuse Radiation, July 13

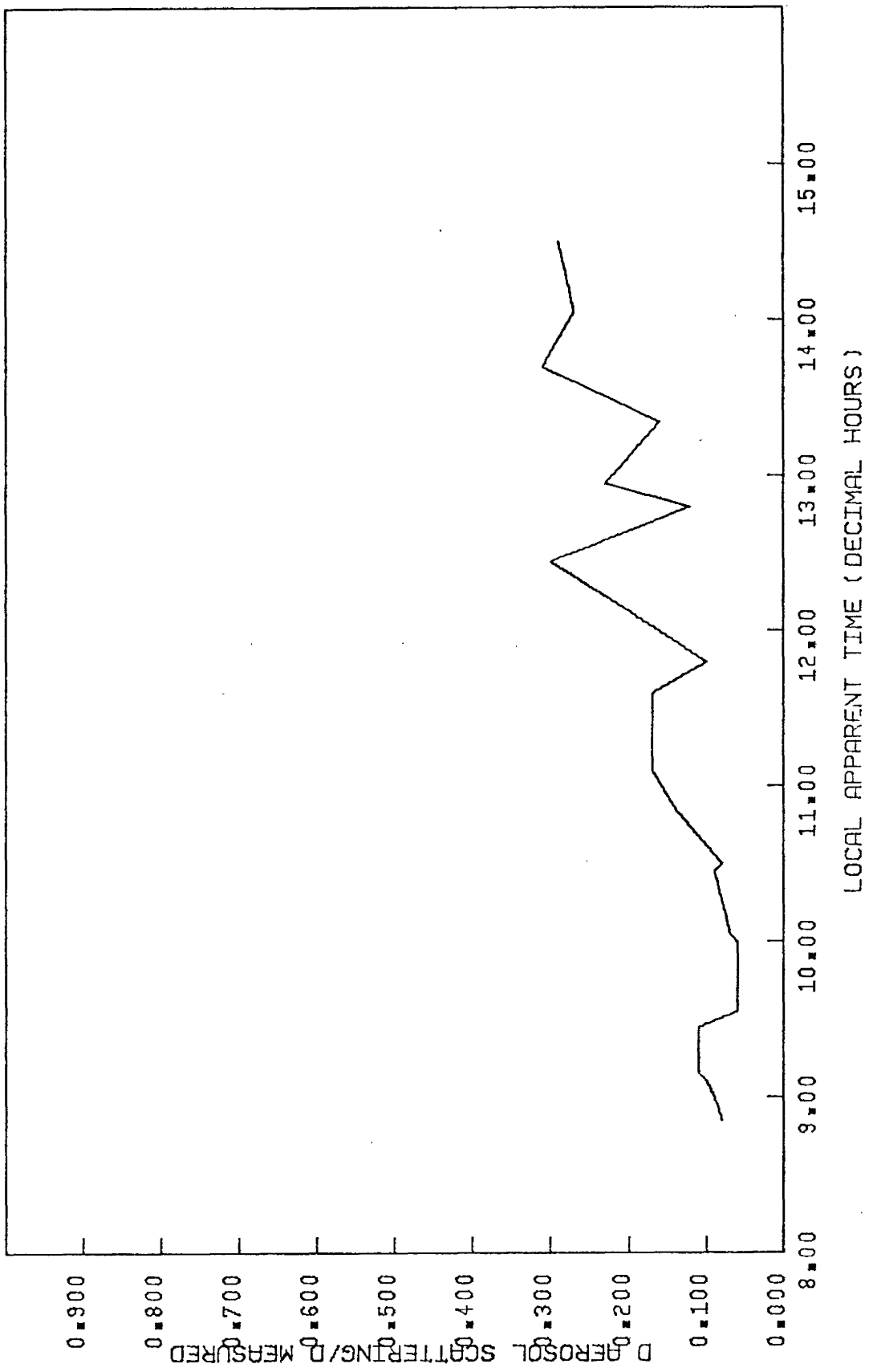

FIGURE 32: Aerosol Scattering Component of Diffuse Radiation, August 1

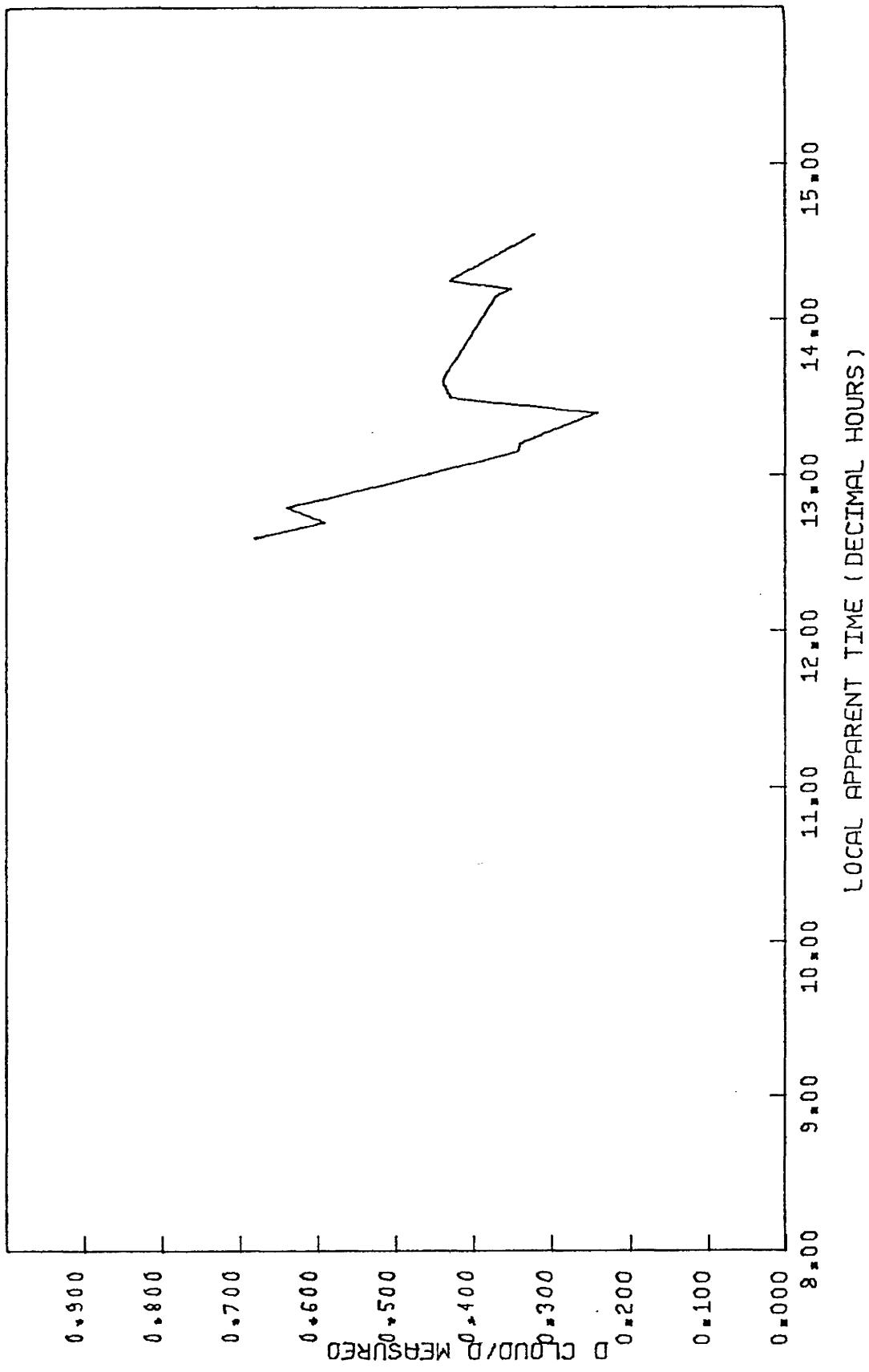

FIGURE 33: Cloud Component of Diffuse Radiation, July 8

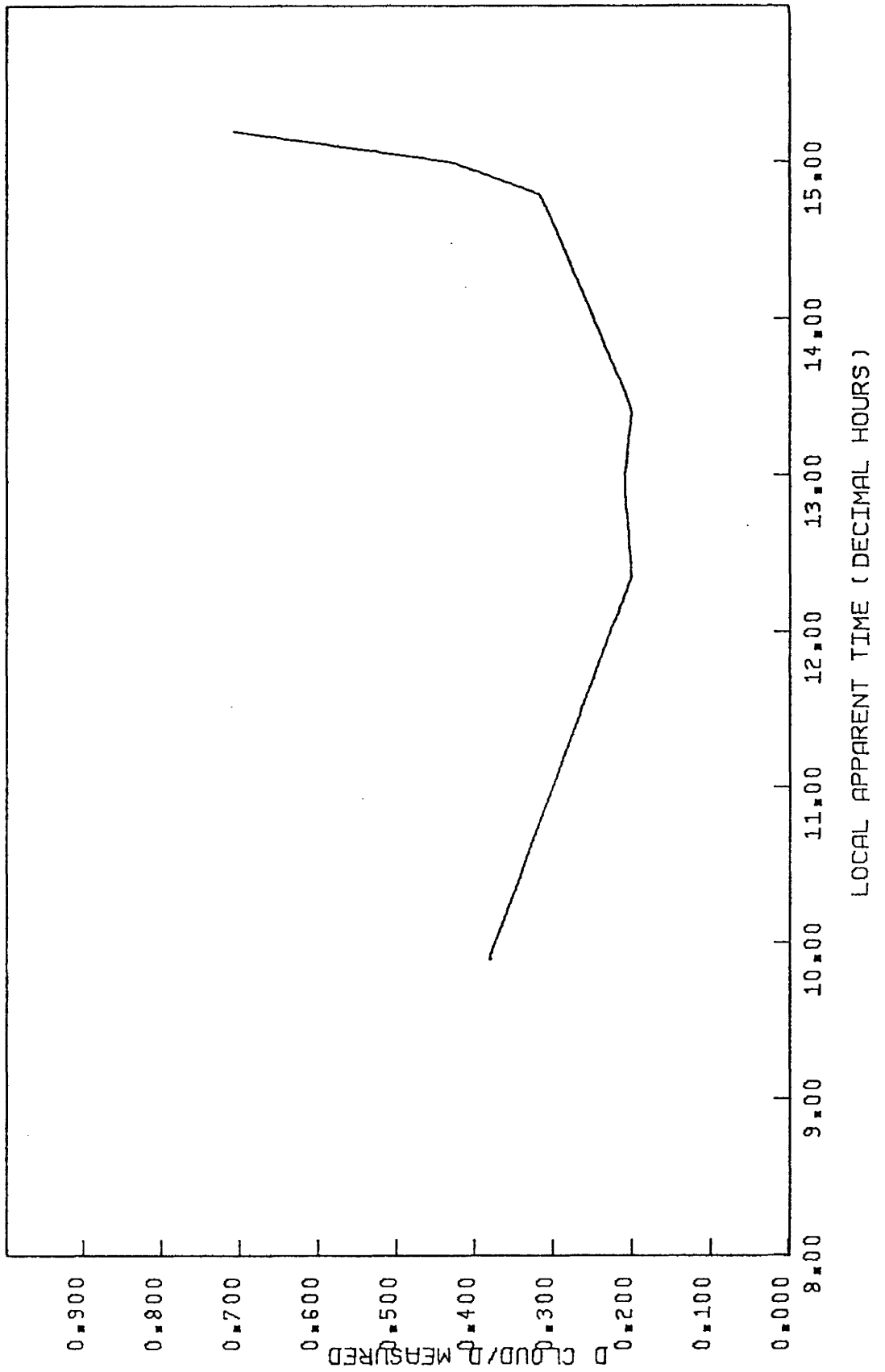

FIGURE 34: Cloud Component of Diffuse Radiation, July 9

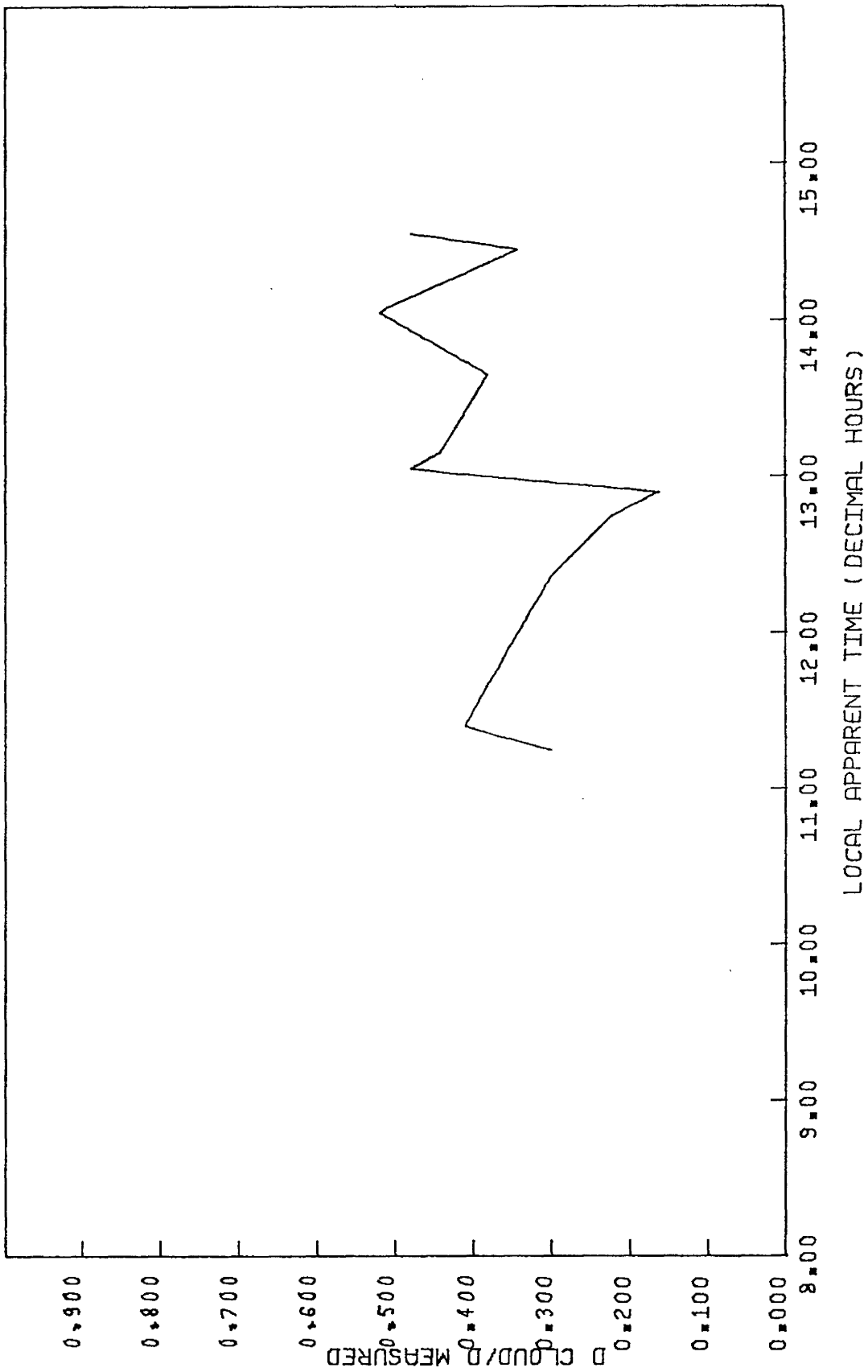

FIGURE 35: Cloud Component of Diffuse Radiation, July 13

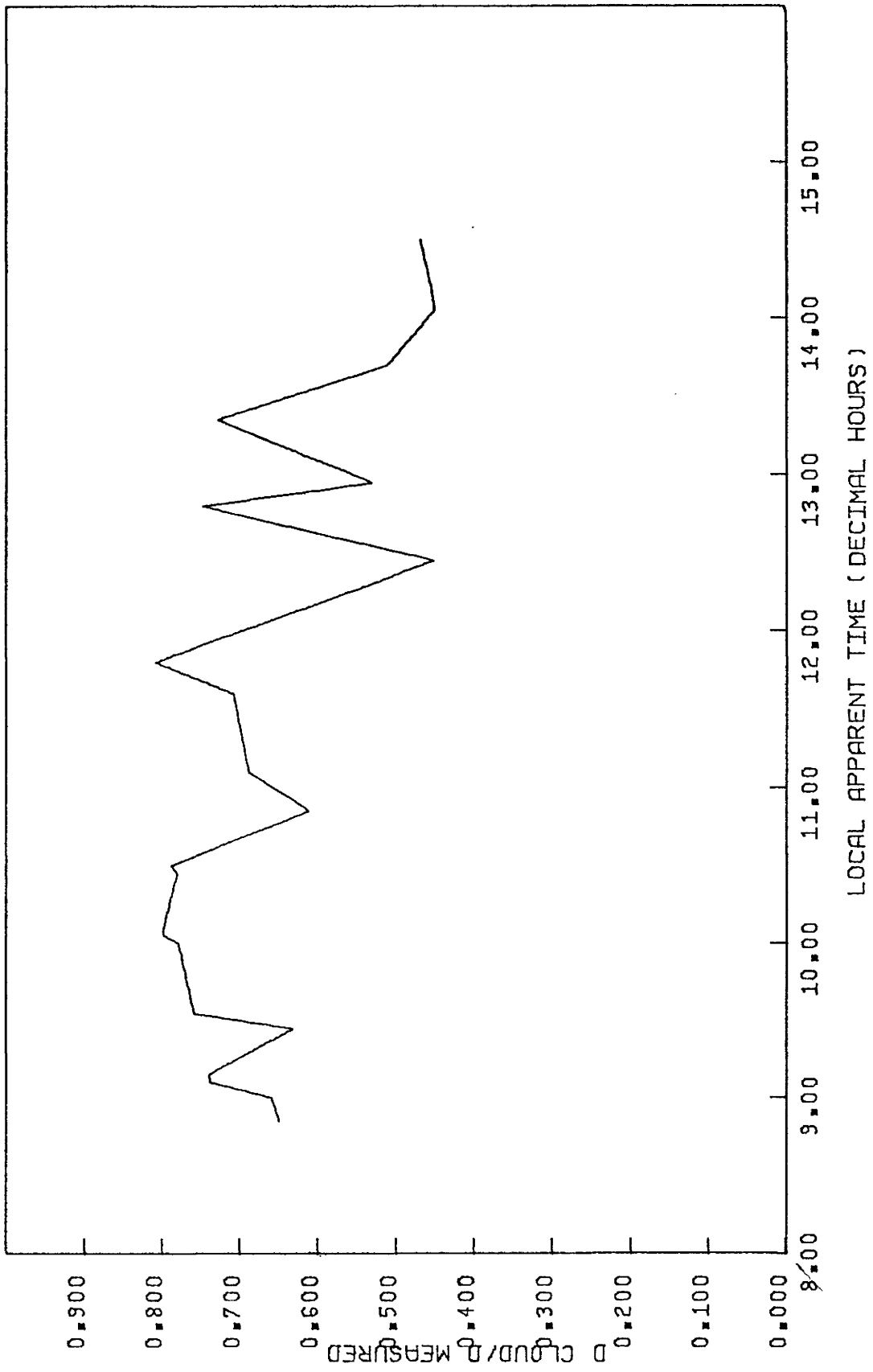

FIGURE 36: Cloud Component of Diffuse Radiation, August 18

controlled by aerosol scattering.

The magnitude of the cloud component also changes with the cloud field. The plot of $D\downarrow_c/D$ for July 9 illustrates this very well. Early in the measurement period (0970 LAT) the cloud field was recorded as 3/10 with $D\downarrow_c/D = 0.26$. The cloud field then decreased to 2/10 at 1290 LAT as the $D\downarrow_c/D$ decreased to 0.14. An increase to 5/10 cumulus cloud cover then followed for the duration of the measurement period and the ratio of $D\downarrow_c/D$ increased to 0.55. Similarly, changes in the aerosol amount over the day will influence the magnitude of the aerosol component. Data for August 18 provides a good example, where both aerosol content and the ratio of $D\downarrow_{as}/D$ progressively increase over time as the ratio of $D\downarrow_c/D$ decreases. A similar trend occurs on July 9 where τ_a and the diffuse component due to aerosol scattering both reach a maximum while $D\downarrow_c/D$ is at a minimum.

E. The Diffuse Flux When the Sun is Obscured by Cloud

In principle, when the sun is obscured by cloud, all of the global solar radiation should be diffuse. Due to the data logger scanning interval of ten seconds, a zero value for direct beam radiation may not be recorded. To compensate for this, all readings of 10 Wm^{-2} or less of direct beam radiation were used since the magnitude of this flux is close to zero; the remainder of $K\downarrow$ being diffuse.

The components of diffuse radiation can be estimated under an obscured sun. If $\Delta D\downarrow$ is the change in the measured diffuse radiation between obscured $D\downarrow$ and unobscured $D\downarrow(0)$ states then $\Delta D\downarrow = D\downarrow - D\downarrow(0)$. It follows that the quantity represented by $\Delta D\downarrow$ is due partly to changes

in both Rayleigh scattering and aerosol scattering but mostly to changes in cloud. Since the time interval between the unobscured and obscured states is small, varying from a few seconds to a maximum of a few minutes, it may be assumed that only the spatial distribution of the cumulus cloud changes while the actual cloud amount remains constant. Hence, the change in diffuse radiation between unobscured and obscured states due to Rayleigh scattering is zero. Therefore, the change in the diffuse radiation $\Delta D\downarrow$ may be evaluated from the expression

$$\Delta D\downarrow = \Delta D\downarrow_c + \Delta D\downarrow_{as} \tag{11}$$

where: $\Delta D\downarrow_c$ = the change in diffuse radiation due to cloud

$\Delta D\downarrow_{as}$ = the change in diffuse radiation due to aerosol scattering

By definition

$$\Delta D\downarrow_{as} = D\downarrow_{as}(0) - D\downarrow_{as} \tag{12}$$

where $D\downarrow_{as}(0)$ and $D\downarrow_{as}$ are the diffuse radiation fluxes due to aerosol scattering in unobscured and obscured skies respectively. Values of $D\downarrow_{as}$ were calculated from

$$D\downarrow_{as} = \frac{D\downarrow_{as}(0)}{D\downarrow(0)} \quad D\downarrow \tag{13}$$

where $D\downarrow(0)$ and $D\downarrow$ are the diffuse solar radiation values under unobscured and obscured sky conditions. Empirical work by Weseley et al. (1976) shows that 60-75% of the direct beam attenuation caused by aerosols is

recovered as an increase in diffuse radiation beneath the cloud layer. Each of the calculated values from equations 11, 12 and 13 were combined to evaluate the cloud effects during the obscured state, where

$$D\downarrow_c = D\downarrow_c(0) + \Delta D\downarrow - \Delta D\downarrow_{as} \quad (14)$$

and $D\downarrow_c(0)$ is the diffuse radiation due to cloud in the unobscured state. Figure 37 illustrates the salient differences between the two states of the atmosphere as referenced in Section B.

Investigation of the obscured state with respect to diffuse radiation enables comparisons to be drawn between that and the unobscured state. Since ΔD_{rs} is assumed zero, the apparent differences are due to cloud and aerosol effects. Figures 38-41 show the difference in the cloud component between the two states. It is noteworthy that the cloud component has a greater influence in the obscured state where, theoretically, all radiation reaching the ground is diffuse. For each day, values of $D\downarrow_c$ exceed $D\downarrow_c(0)$ as expected; the magnitude depending on the cloud field, cloud density and length of time that the sun is obscured. The data show that clouds exert a substantial effect on the diffuse flux often leading to substantial increases in radiation. In fact, the effect of cloud may be great enough (with the added effects of multiple scattering) to allow a larger radiation flux than under clear skies.

The aerosol component of diffuse radiation is less simple. Values of $D\downarrow_{as}$ and $D\downarrow_{as}(0)$ were compared for each of the measurement days. Results do not indicate any convincing trends except for the fact that the contribution of the aerosol term is less than the cloud term for the

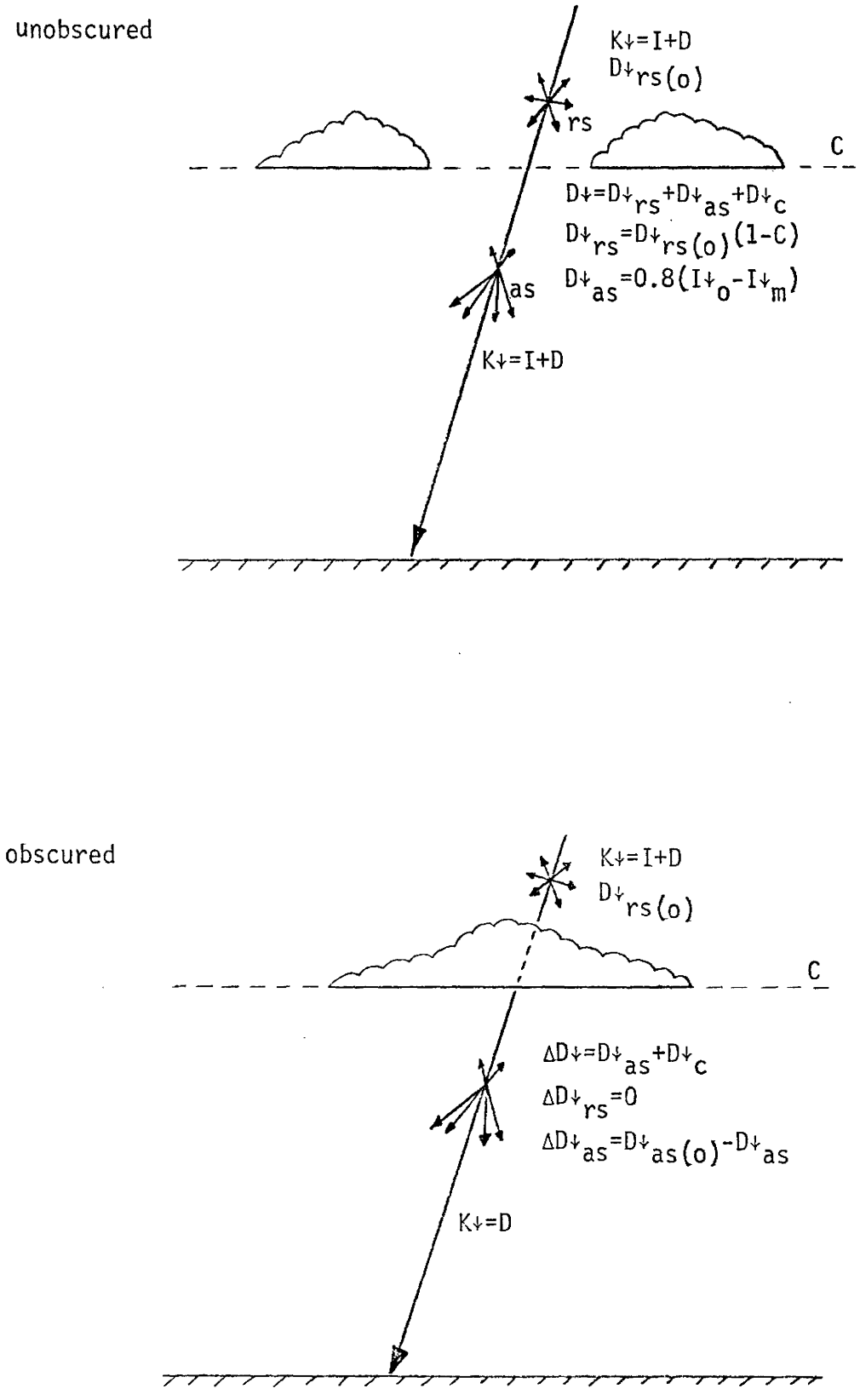

FIGURE 37: Schematic diagram of unobscured and obscured sky conditions.

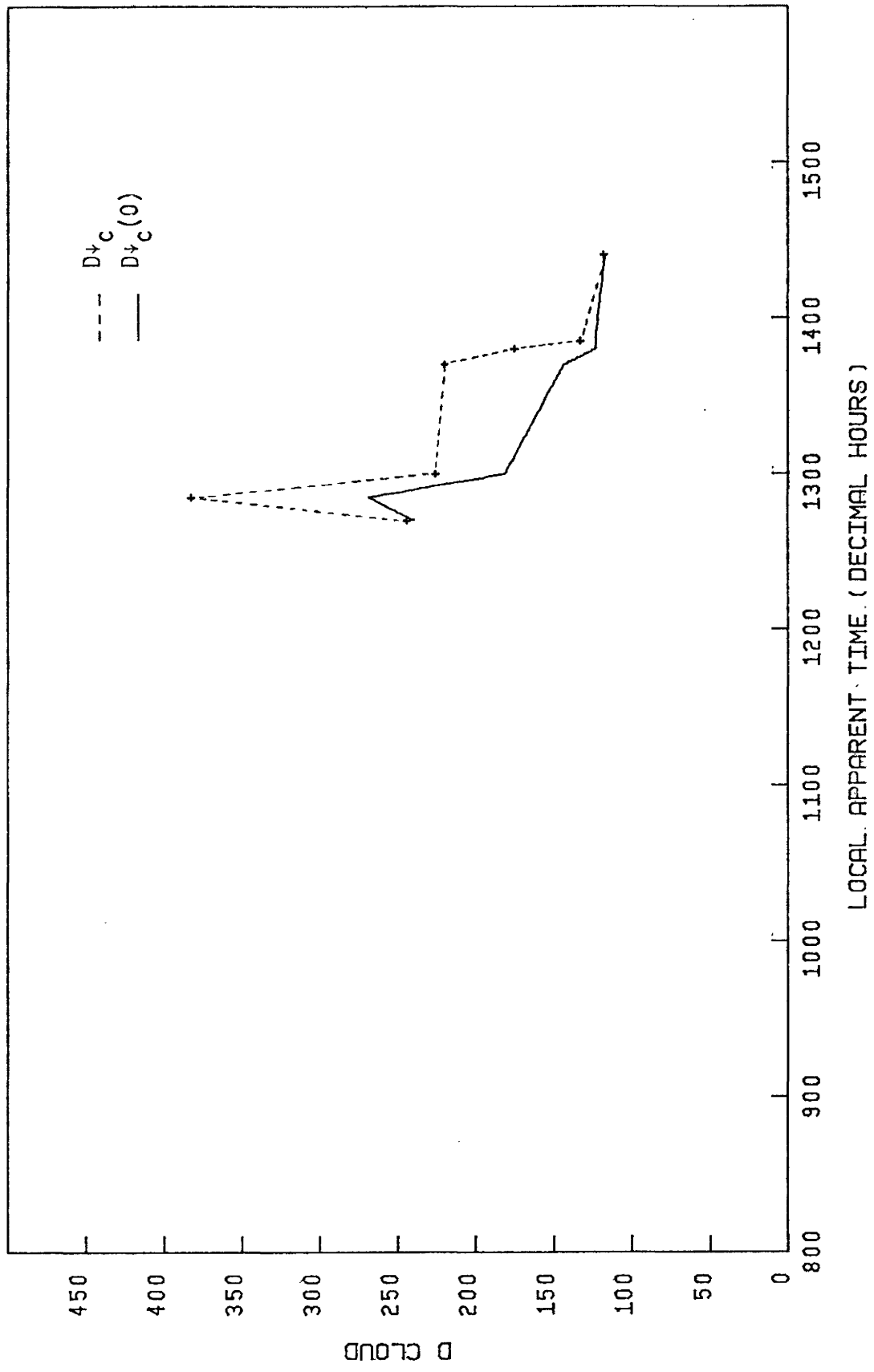

FIGURE 38: Change in the cloud component between unobscured and obscured states, July 8

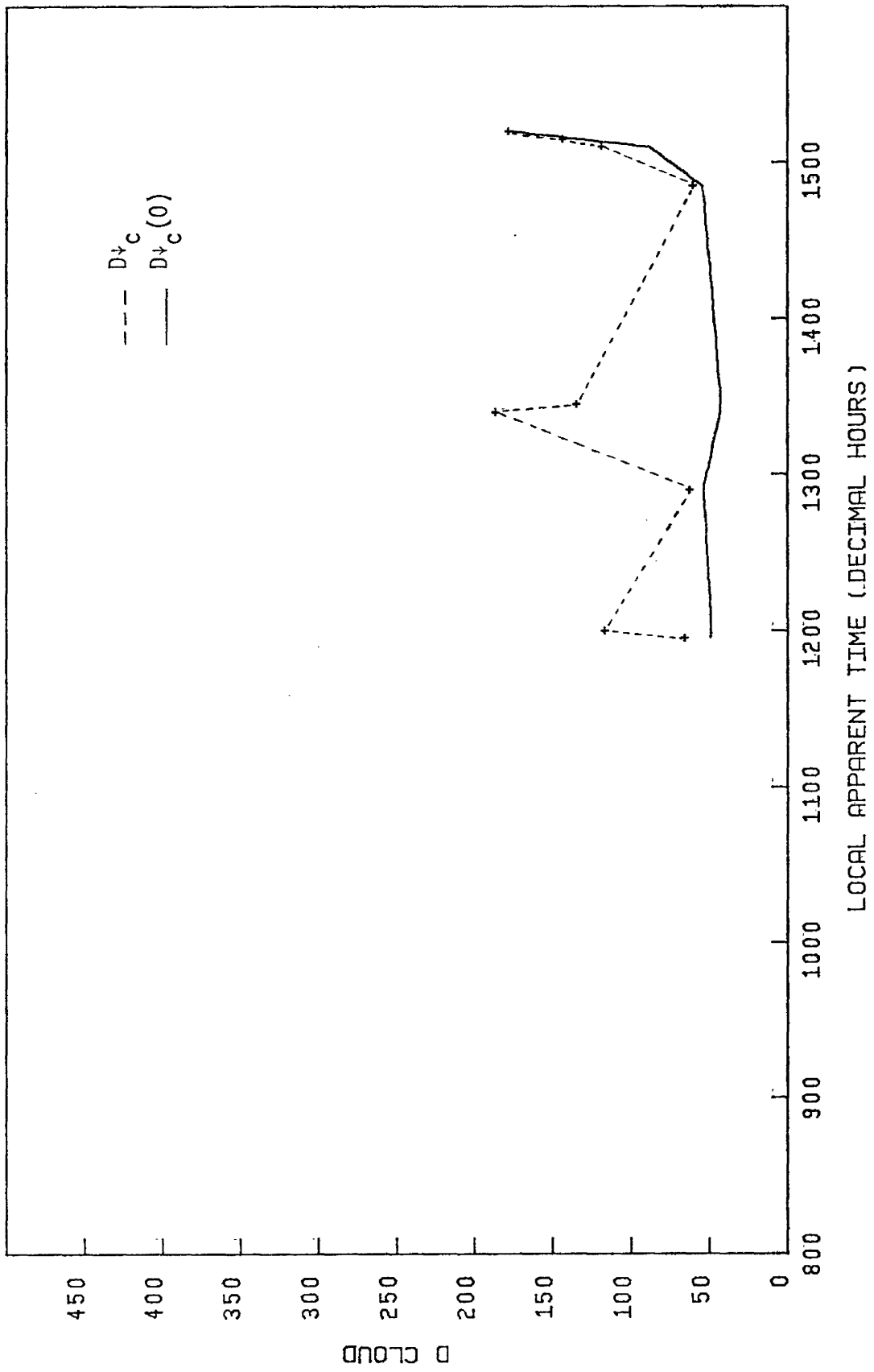

FIGURE 39: Change in the cloud component between unobscured and obscured states, July 9

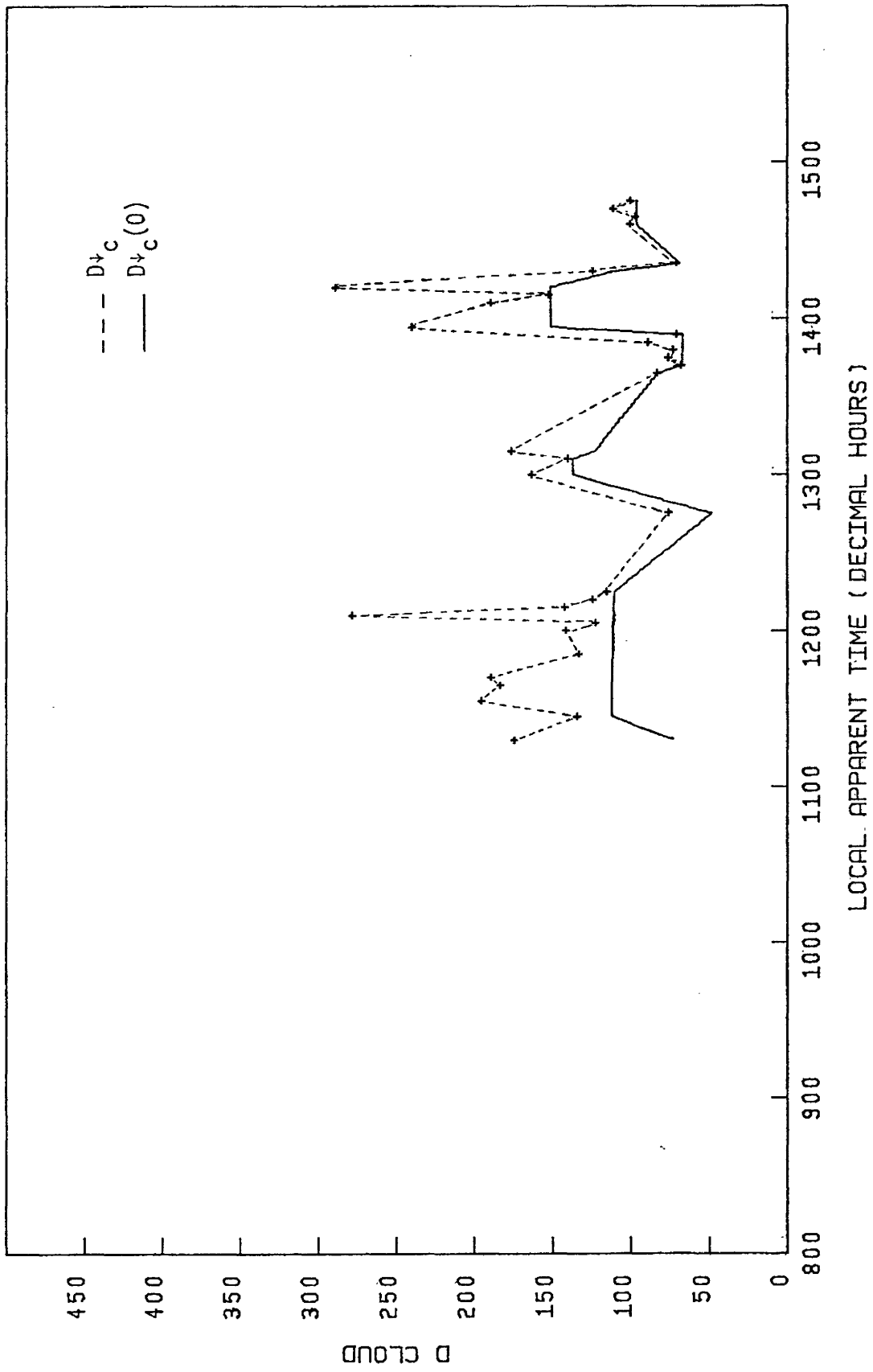

FIGURE 40: Change in the cloud component between unobscured and obscured states, July 13

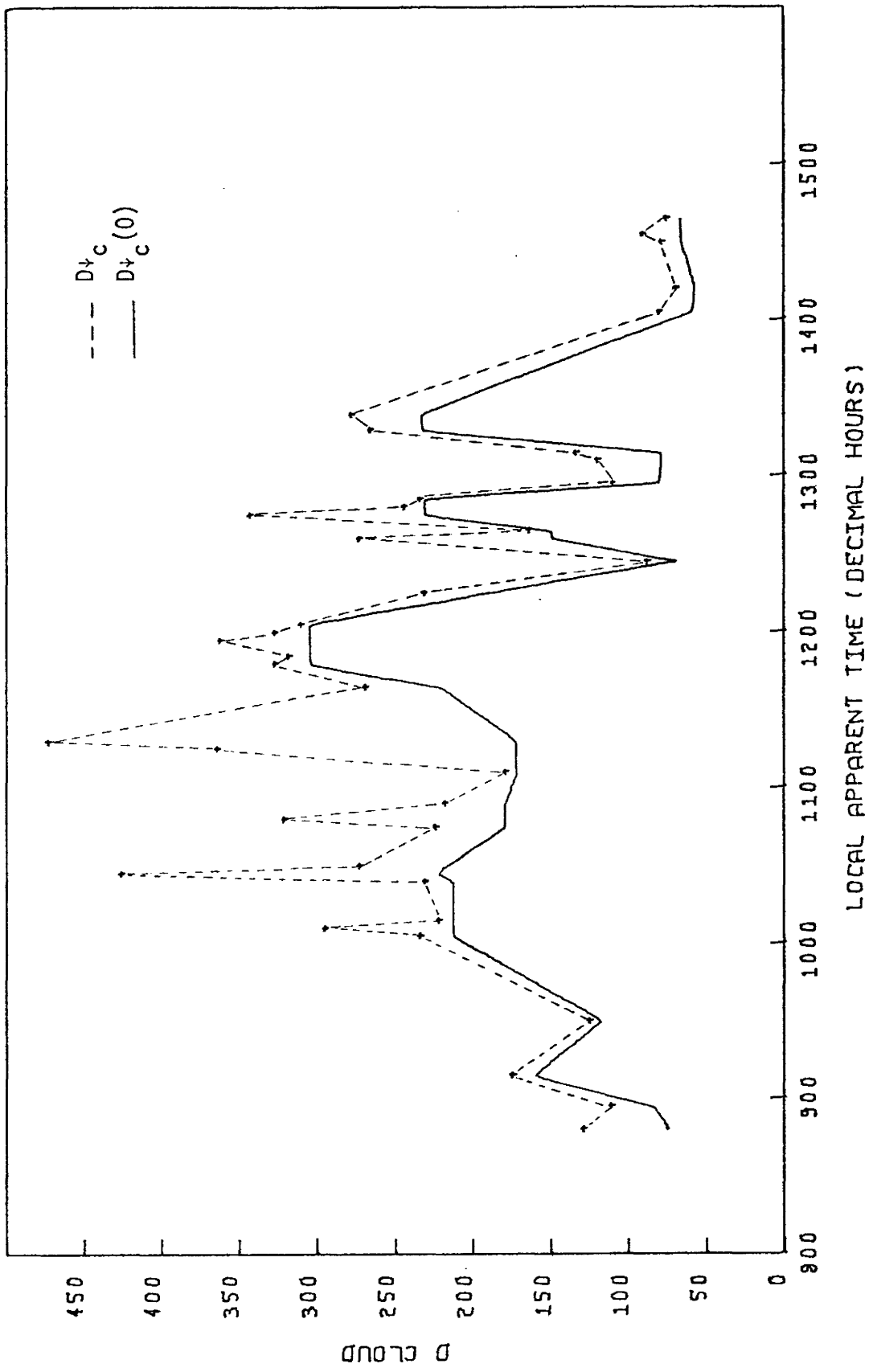

FIGURE 41: Change in the cloud component between unobscured and obscured states, August 18

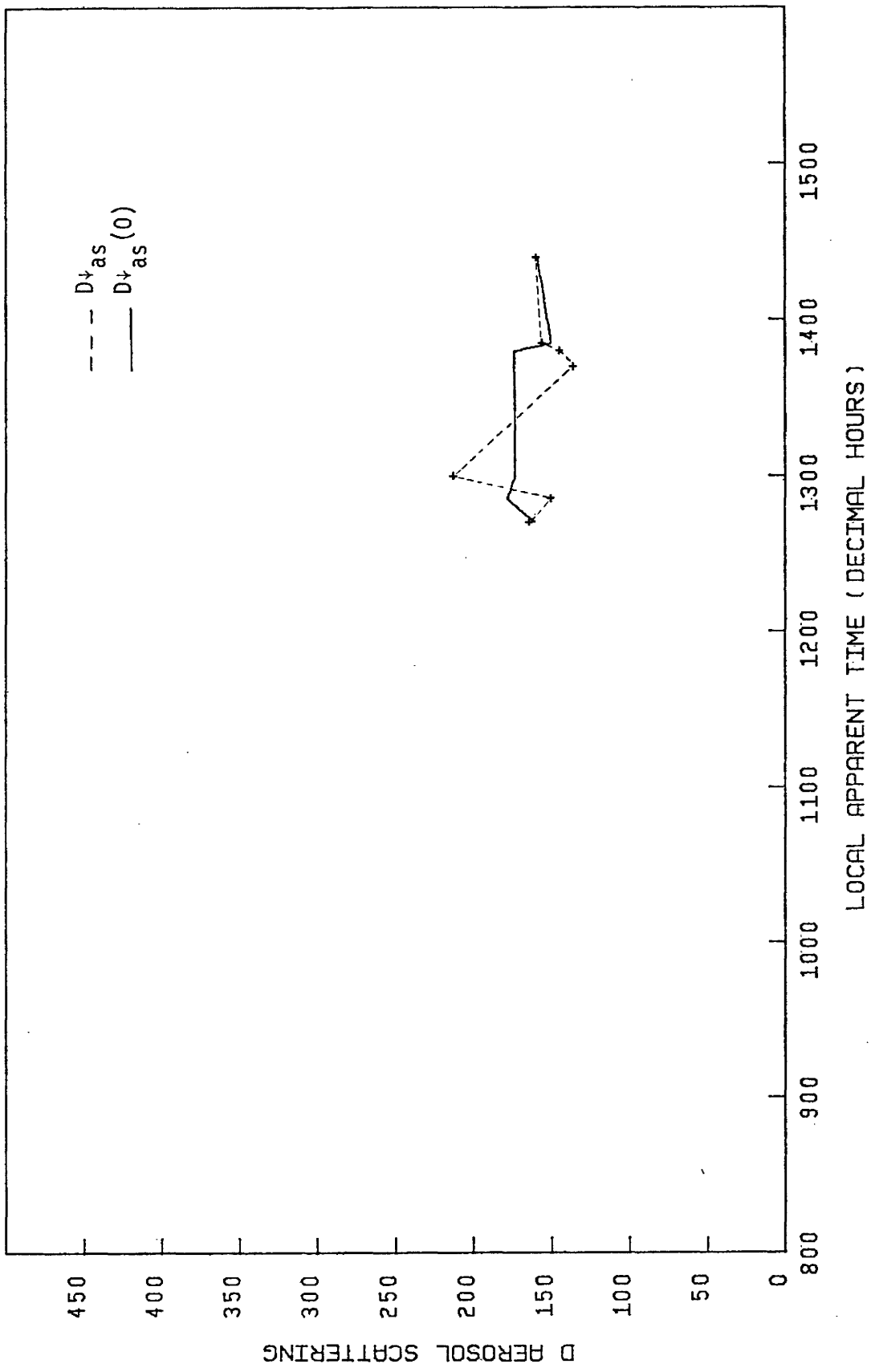

FIGURE 42: Change in the aerosol component between unobscured and obscured states, July 8

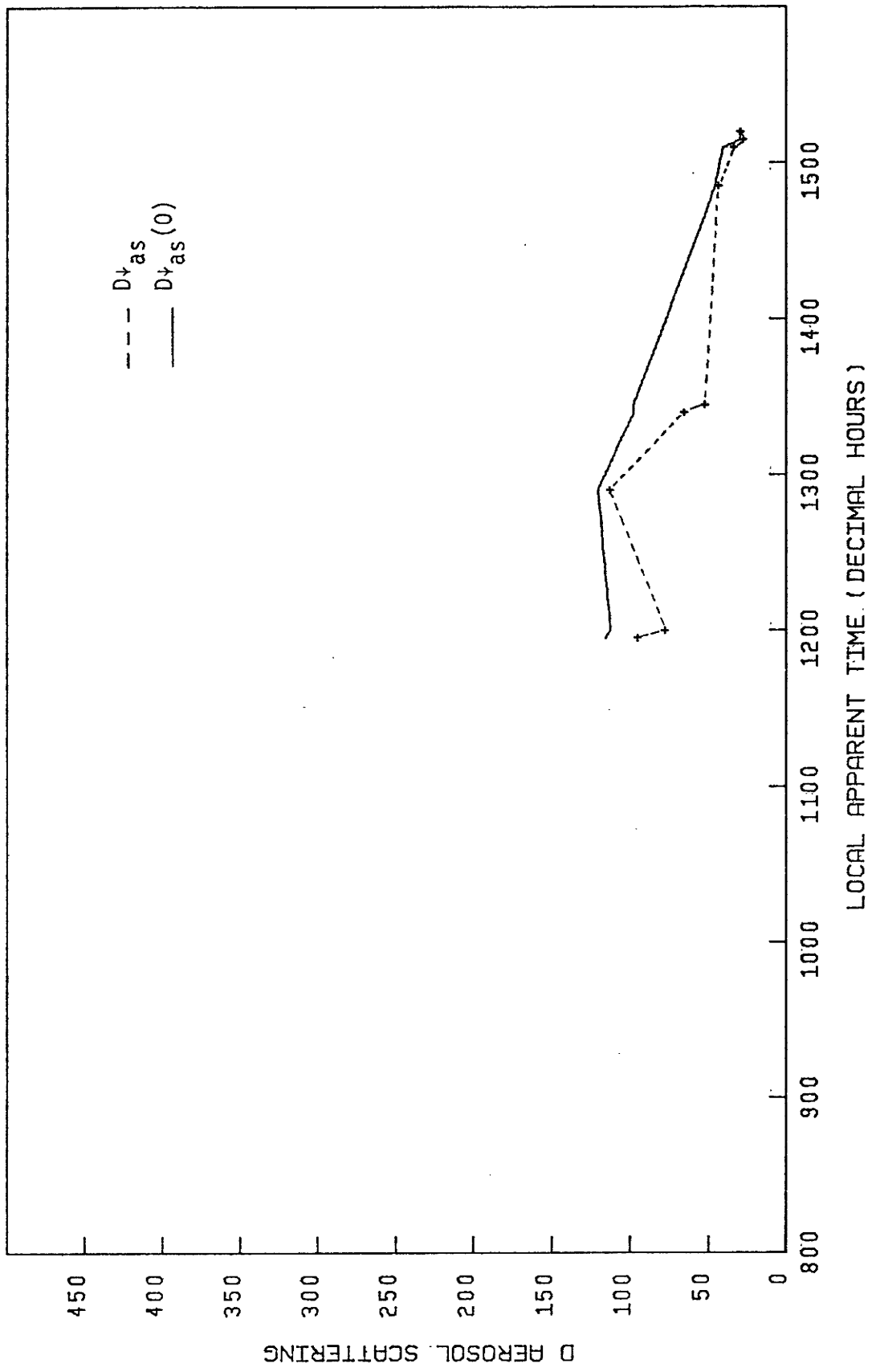

FIGURE 43: Change in the aerosol component between unobscured and obscured states, July 9

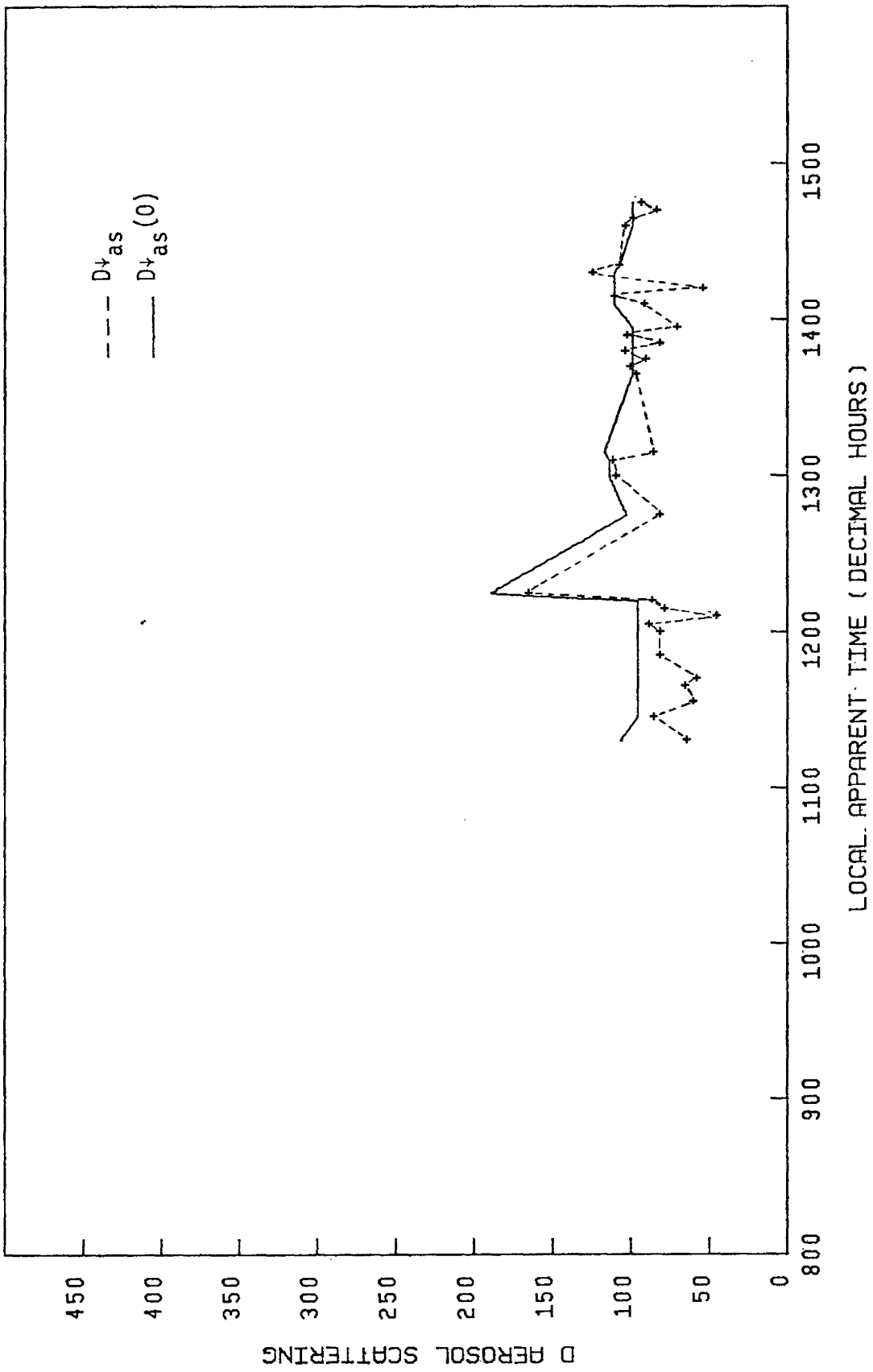

FIGURE 44: Change in the aerosol component between unobscured and obscured states, July 13

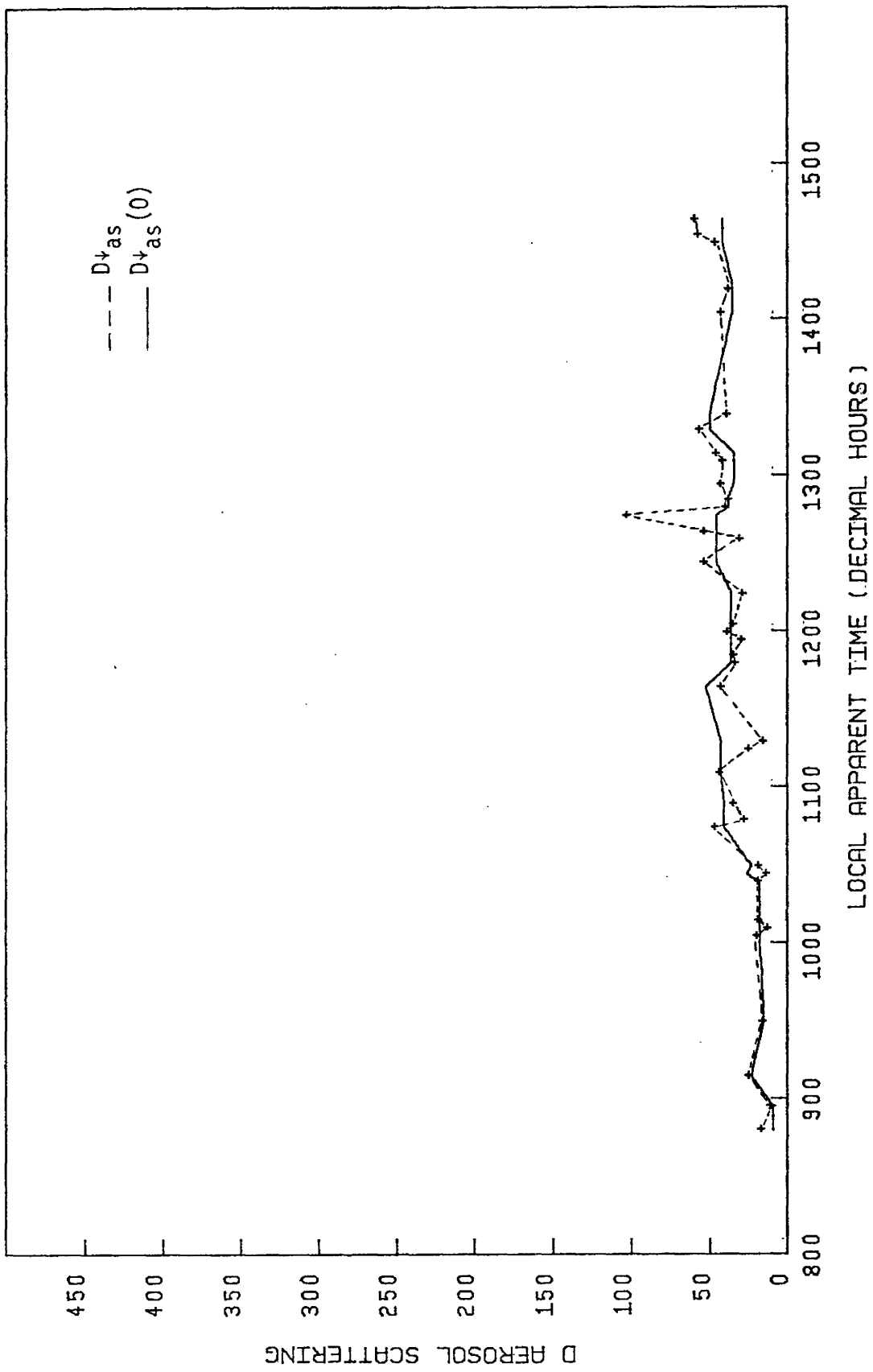

FIGURE 45: Change in the aerosol component between unobscured and obscured states, August 18

obscured state. Figures 42-45 indicate the fluctuating behaviour of $D\downarrow_{as}$ with respect to $D\downarrow_{as}(0)$ which is particularly visible in the plot for August 13. There is no consistency in the data on this day and it appears that clouds have no effect on the aerosol term. Plots for July 8, 9 and 13 suggest that values of $D\downarrow_{as}$ are generally less than $D\downarrow_{as}(0)$. Regardless of what argument is accepted, $\Delta D\downarrow_{as}$ may assumed to be very small in contrast to values of $\Delta D\downarrow_{c}$ for the same time periods. Values of the Monteith and Unsworth turbidity factor which rely upon measured and theoretical values of direct beam radiation do not apply to the obscured state, since direct beam radiation is zero.

F. Synoptic Summaries for Measurement Days

Information regarding local weather conditions was obtained from the Surface Weather Records at Mount Hope Airport and supplemented with data extracted from computer plotted maps of Canada at the Ontario Weather Centre, Toronto. The Great Lakes region has been extracted from each of these maps and simplified to include isobars, high and low pressure cells and fronts. This information appears in Figures 46-53. The following outlines the salient weather for each day:

July 8 0600Z: a low pressure cell was located over Lake Ontario as well as an occluded front as cool air entered the region from the northwest, met a warm air mass and pushed it southward. The Great Lakes region experienced extensive cloud cover.

July 8 1200Z: the occluded front weakened as the low pressure cell moved slowly to the northeast being replaced by cool air behind the cold front advancing from the northwest. Cloudiness was reduced.

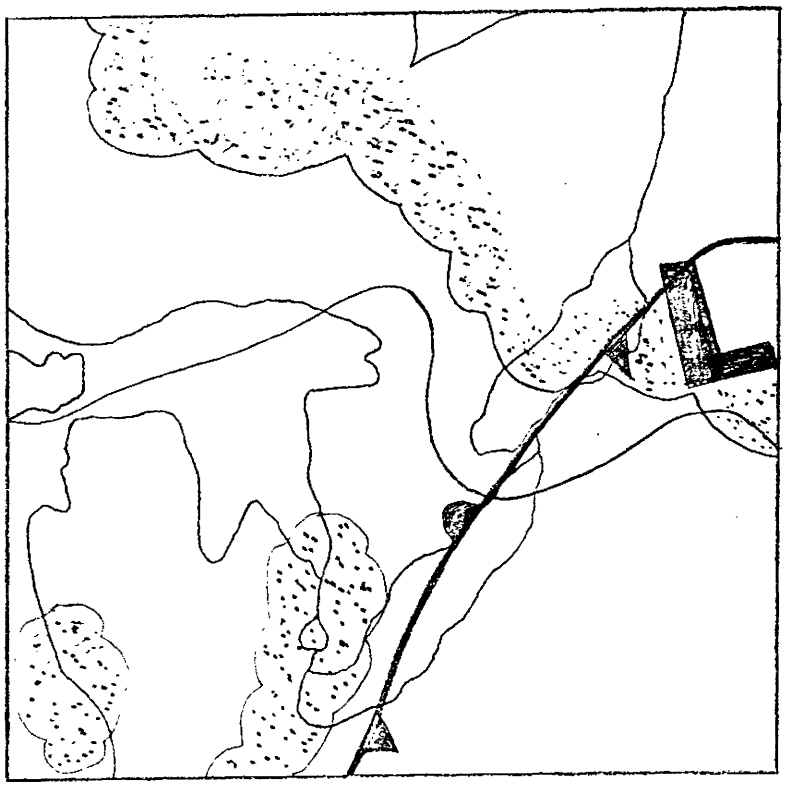

FIGURE 46: Synoptic situation, July 8: 1200Z

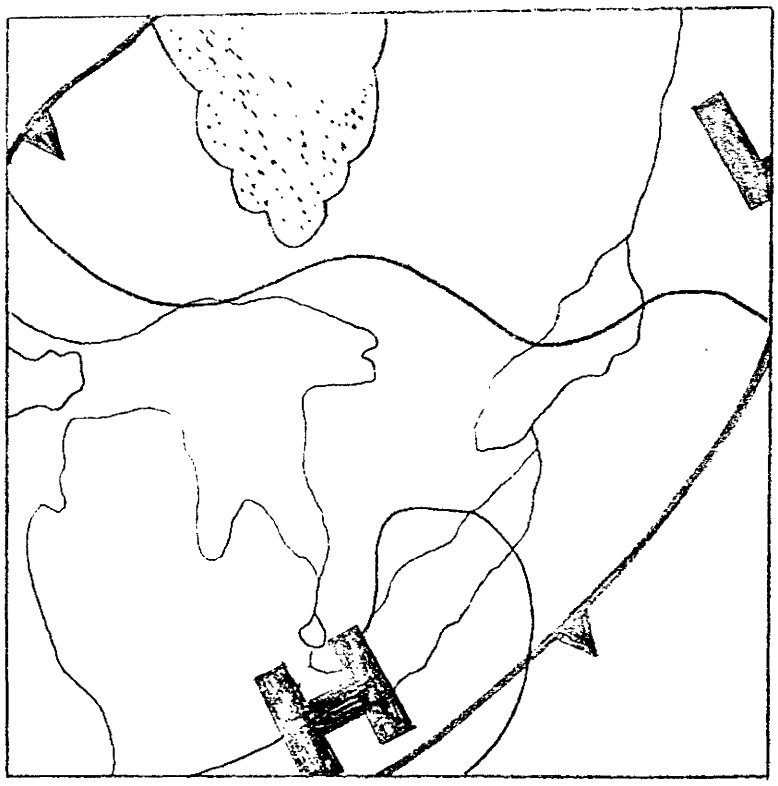

FIGURE 47: Synoptic situation, July 8: 1800Z

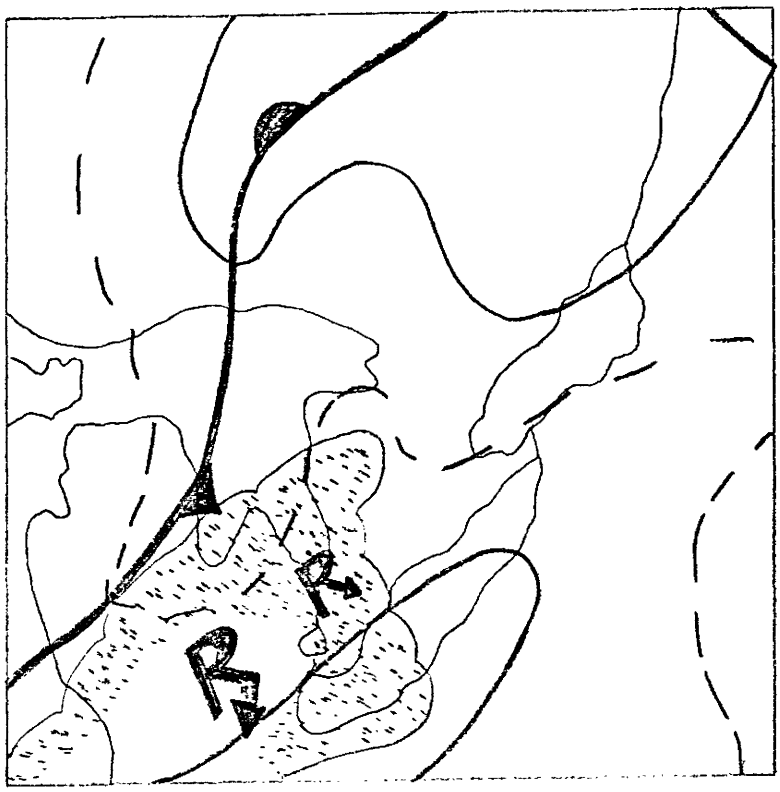

FIGURE 48: Synoptic situation, July 9: 0000Z

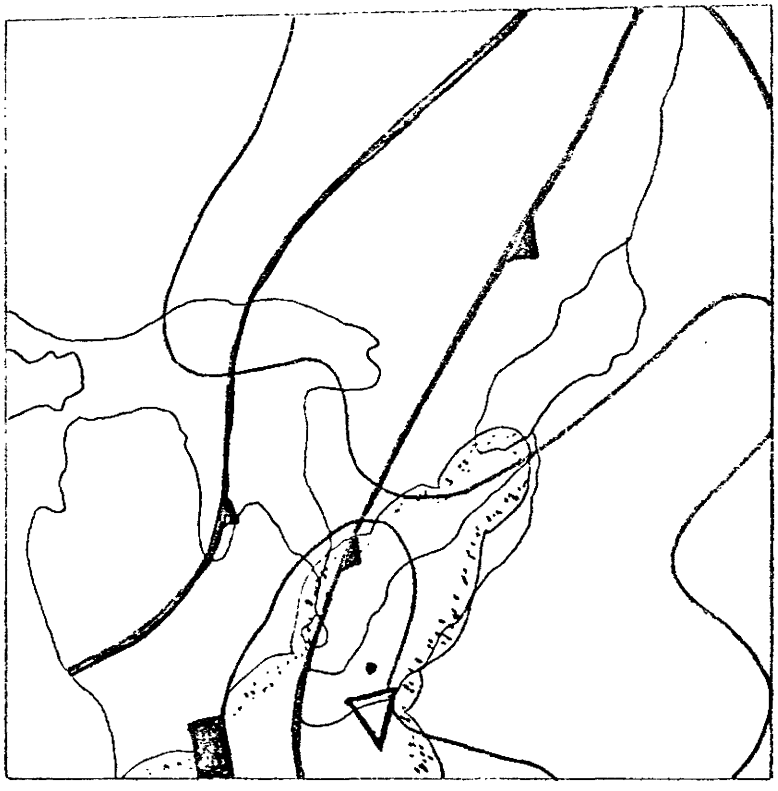

FIGURE 49: Synoptic situation, July 9: 0600Z

FIGURE 50: Synoptic situation, July 9: 1200Z

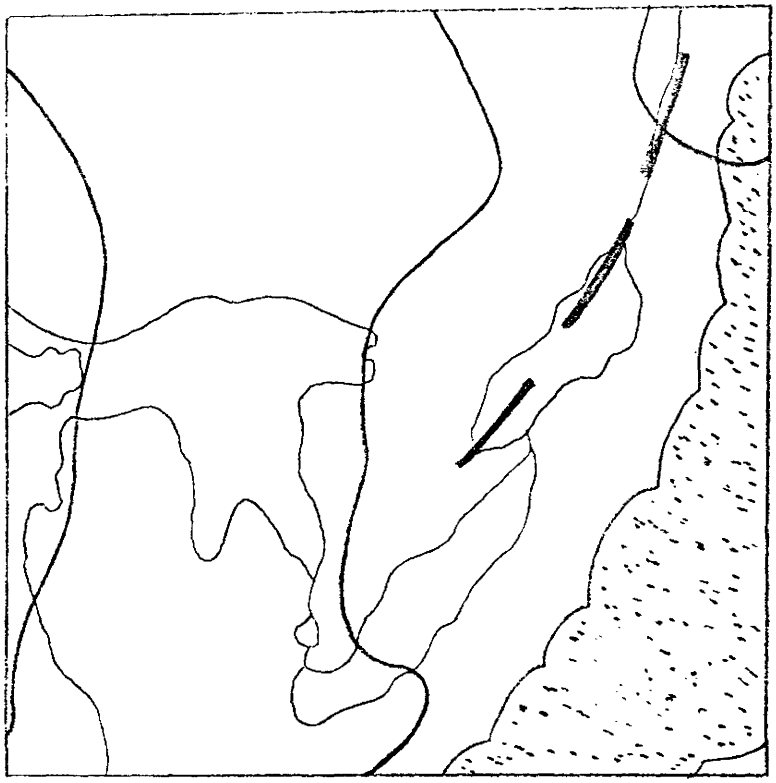

FIGURE 51: Synoptic situation, July 9: 1800Z

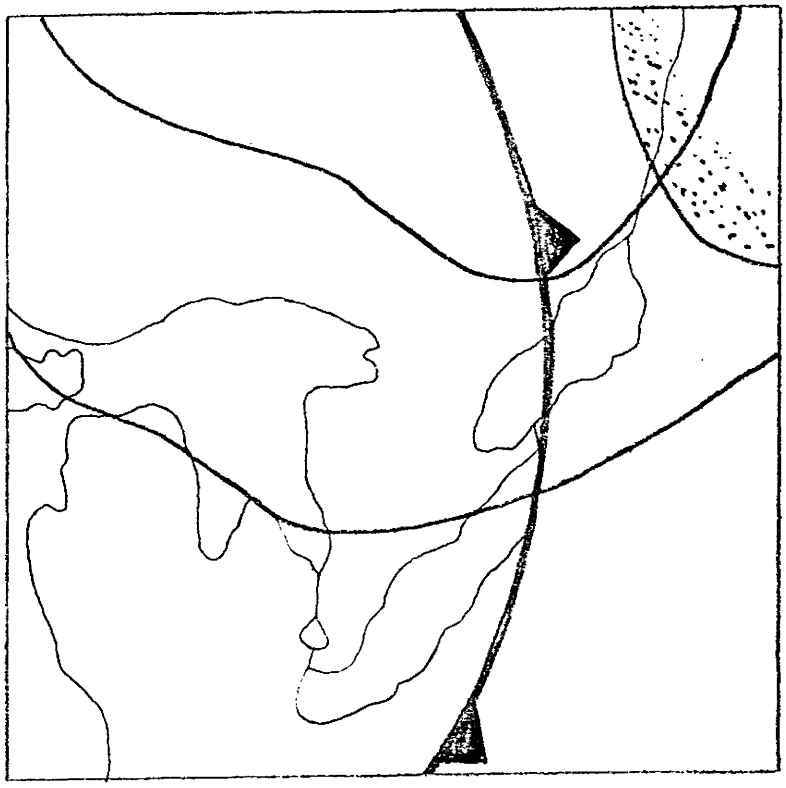

FIGURE 52: Synoptic situation, July 13: 1200Z

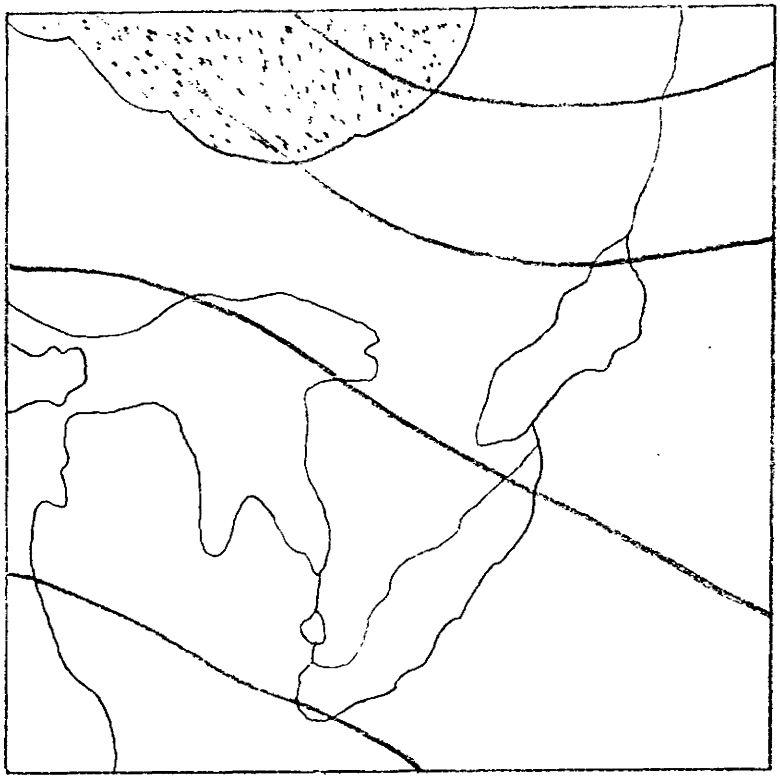

FIGURE 53: Synoptic situation, August 18: 1200Z

July 8 1800Z: occluded front has now moved northwest and a high pressure cell was centred along the south shore of Lake Erie. The cold front cited at 1200Z was stationary and the area was cloud-free.

July 9 0000Z: the cold front separated a warmer air mass which moved in a northeasterly direction. A trough of low pressure extended from the southeastern U.S.A. up through Hamilton with thunderstorm activity over Southern Lake Erie and Southern Lake Huron.

July 9 0600Z: clear skies prevailed as the occluded front continued to move northeastward and a cold front moved in from the northwest. A high pressure cell slowly advanced from the west.

July 9 1200Z: cold front was located over Hamilton and cloud patches developed along the Lake Ontario shore. A high pressure cell approached Lake Superior.

July 9 1800Z: The area was influenced by a trough of high pressure as the high pressure cell moved eastward. Wind direction was from the northwest.

July 10 0000Z: the entire Great Lakes region was influenced by the high pressure cell.

July 13 1200Z: winds were from the southwest and a cold front was located over Lake Ontario.

August 18 1200Z: a high pressure cell influenced the Great Lakes area. This cell replaced the cold front which was now over the Atlantic coast.

G. Other Work

Idso (1970) has considered the transmittance of the atmosphere for solar radiation on individual clear days at Phoenix, Arizona. Following Houghton (1954), Idso defined transmittance of the atmosphere as a function of absorption and scattering by each of: water vapour, dust (aerosol) and dry, dust-free air (Rayleigh). He showed that daily averages of atmospheric transmittance could be calculated to within 1.5% of measured values, assuming the aerosol content was constant; thus transmission was

specified by only one meteorological variable, precipitable water. These assumptions appeared to be operationally valid yielding a correlation coefficient of 0.92 between measured and calculated transmittances. Only 17 of the 100 total observations fell outside the 1.5% interval from the 1:1 line.

Robinson (1966) briefly considered the influence of clouds on global solar radiation, pointing out their complex nature and noting that cumulus clouds are darkest when just in front of the sun, and have a very bright borderline, although as a whole they appear brightest when opposite to the sun.

Work by Kondratyev (1969) calculated the percentage of solar radiation transmitted as the ratio of the observed flux in the presence of cloud obscuring the sun to that in a cloudless sky. The latter was determined from interpolation over actinographic recordings. The author does not present values for cumulus cloud, but does indicate altocumulus transmission ranges for different solar heights. Results indicate that for solar heights 5-15°, 15-25° and 25-35°, maximum and minimum transmissions are 14-7%, 20-1% and 37-2% respectively. Kondratyev points out that these results are approximate, in view of the limited number of observations and the method used to determine them. He further notes that transmission values depend largely upon the amount and form of cloud cover, where transmission of radiation decreases as the clouds reach greater vertical extent. Conversely, cloud albedo shows an increase with cloud thickness.

The absorption, reflection and transmission of solar radiation in cloudy skies has been investigated by Liou (1976) as he performed band calculations over the entire spectrum. He confirms generalities pre-

viously mentioned, but points out that clouds also emit thermal infrared radiation according to their temperature. The transfer of radiation through cloud depends on the particle phase, concentration, size and distribution and on cloud thickness. Evidence from this study indicates that cloud location in the sky is important in determining the absorption of solar radiation, while the optical pathlengthis determined by thickness and composition of the cloud as well as the solar zenith angle. Transmission values were derived: when the sun was overhead, cumulus clouds transmitted 20% of the radiation incident upon them. Owing to the increased atmospheric pathlength, transmission decreases as the sun moves toward the horizon. Reflection of cumulus cloud with a thickness of 0.45 km was 63-85%, but the absorption was only 4-9%.

A study by Robinson (1977) yielded ground-based measurements of total global solar and direct beam radiation when isolated, approximately cubic cumulus clouds were present. In general, transmission through cloud has been shown to be inversely proportional to cloud thickness; since Robinson has only considered small, cubic cumulus, the total downward radiation emanating from a cloud is almost constant, irrespective of thickness. The method of data collection was similar to that at the McMaster site, where incoming global radiation was measured with an Eppley Precision Spectral Pyranometer and direct beam with a Normal Incidence Pyrheliometer. Diffuse radiation was calculated by residual from ($K\downarrow$ - IcosZ). Cloud photographs were taken and inferences regarding atmospheric conditions were made from airport observations and radiosonde ascents. Owing to the selectivity of Robinson in choosing this special form of cloud (where lateral development is implied to equal vertical development, which is

minimal), he reports unusually high transmittances ranging from 74-92%.

Finally, Monteith (1973) has observed that immediately prior to and following the period when the sun is obscured by cloud there is a significant increase in measured K↓ that has been known to reach 100 Wm^{-2} in temperate latitudes. Atmospheric conditions on July 9 were characterized by the presence of single, isolated cumulus clouds, which allowed the detection and analysis of Monteith's observation. Examples of this phenomenon at the McMaster site are tabulated here:

Time Interval	Increase in K↓ prior to cloud (Wm^{-2})	% increase	Increase in K↓ after cloud (Wm^{-2})	% increase
111830-111950	20	2.3	102	12.8
134500-134610	1	0.1	2	0.2
142020-142220	1	0.1	185	21.7
144720-144820	5	0.6	255	41.1
160740-161050	3	0.4	192	32.6

It is noteworthy that the increase in radiation is always greater following the period when the sun is obscured by cloud. Monteith (1973) attributed this increase in radiation to strong forward scattering by water droplets near the edge of the cloud.

CHAPTER V

CLOUDLESS SKY SOLAR RADIATION

A. Calculation of Precipitable Water

In order to draw inferences regarding the effect of cloudy conditions on solar radiation fluxes, theoretical, cloudless sky values for an aerosol-free atmosphere were calculated. The model values were calculated from the 1200 GMT radiosonde ascent at Buffalo International Airport (see Appendix 1). These data were used to obtain precipitable water from

$$W = \frac{1}{g} \int_{P_o}^{P_z} q \, d \, P \tag{15}$$

where: g = acceleration due to gravity ($9.81\ ms^{-2}$)

q = specific humidity

P = pressure

and the subscripts z and o indicate the top of the ascent and the ground surface.

The integral was evaluated numerically from

$$W = \sum_{i=1}^{n} \left(\frac{1}{g} \bar{q}_i \, \Delta P_i\right) \tag{16}$$

where: $\bar{q}_i$ = mean specific humidity for layer i

ΔP_i = change in pressure in layer i

Precipitable water calculations from the Buffalo radiosonde data are given in Appendix 1.

B. Calculation of Cloudless Sky Solar Radiation

A cloudless sky solar radiation model (Davies and Uboegbulam, 1978) for an aerosol-free atmosphere was employed to derive comparable values of radiation fluxes to those measured at the McMaster site. These model values are calculated from latitude and longitude of the site (43° 17'N, 79° 50'W), date, precipitable water, solar declination, equation of time and radius vector.

Calculated cloudless sky solar radiation values are symmetric about solar noon. Calculated values for each day represent the time period when the sun is above the horizon, and consequently shortwave radiation may be estimated. The limits of this period were determined by a subroutine in the computer program. Actual measurement periods overlap a small range of the calculated period. Field measurements have been compared with these values showing that the model over-estimates the direct beam component and under-estimates the diffuse component. These differences are to some degree accentuated by the fact that the model calculations are based on a cloudless, aerosol-free atmosphere. Caution must be taken to distinguish between "true cloudless conditions" that the model predicts and "unobscured sun conditions" meaning unaltered direct beam under actual measurement conditions. It should be noted that measurements were obtained from an atmosphere with aerosols.

C. Cloud Data

The difficulties in obtaining accurate cloud data have been referenced in Chapter 1, but warrant further consideration here. Cloud observations were collected for each of the measurement days at Mount Hope Airport and at the radiation measurement site. Cloud differences between the two sites were usually within one-tenth (see Appendix 2). Cloud fields and sky conditions in general were evaluated in terms of a very coarse qualitative scale which allowed some investigation of vertical and lateral cloud development (little, moderate, extensive), cloud field (in tenths of sky covered) and cloud distribution (small isolated, massive, clusters). Additional data on wind speed were obtained from the Surface Weather Records.

CHAPTER VI

CONCLUSIONS

Cloud transmission values calculated from measurements at McMaster University in 1977 compare favourably with those published by Haurwitz (1945) for the Blue Hill Observatory. Typically, summertime cumulus formed in late morning and often dissipated by late afternoon. Irrespective of cloud amount, these clouds generally transmitted about twenty percent of the solar radiation. Hence, the hypothesis employed that cumulus clouds behave similarly to other "low clouds" was justifiable.

Two states of the atmosphere were defined: an "unobscured" state where the sun was not obstructed by cloud and most of the incoming solar radiation was direct beam and the "obscured" state where the sun was occluded by cloud which diffused the incoming solar radiation. The global solar radiation was substantially reduced in the presence of cloud, but the distribution of radiation over time was strongly bi-modal corresponding to the constant change in cloud position, relative to the sun. The diffuse flux was assumed to be made up of three components: diffuse radiation due to Rayleigh scattering, aerosol scattering and cloud. Rayleigh scattering for the unobscured state was shown to be a function of Rayleigh scattering in a model atmosphere (cloudless, aerosol-free) corrected by a cloud factor. When the sun became obscured by cloud, only the spatial distribution of the clouds was changed, and hence, Rayleigh scattering

was assumed constant over both states. Therefore, the change in the amount of diffuse radiation was evaluated from the changes in diffuse radiation due to cloud and aerosol. The aerosol term was directly related to the Unsworth and Monteith turbidity factor under unobscured conditions. In the case of the obscured state, the cloud component dominated and the aerosol term was suppressed.

Extensive use of on-site and airport cloud observations (as well as on-site cloud photography) provided reliable data on sky conditions for each measurement day. Data from radiosonde ascents were used to calculate precipitable water and theoretical, cloudless, aerosol-free atmosphere radiation fluxes enabling a comparison between the measured and calculated values.

Despite the successful results of this particular study, the major problem of quantitatively assessing cloud behaviour remains. Clouds continue to pose problems in climatic modelling due to their dynamic nature and consequently, field determination of their effects under varying atmospheric conditions remains to be investigated in greater detail.

REFERENCES

Davies, J.A., Schertzer, W. and Nunez, M. (1975) Estimating Global Solar Radiation. *Boundary-Layer Meteorol.*, 9, 33-52.

Davies, J.A. and Uboegbulam, T. (1978) Estimates of the surface incoming radiation for "Quadra" during GATE (submitted paper).

Haurwitz, B. (1945) Insolation in Relation to Cloudiness and Cloud Density. *J. Appl. Meteor.*, 2, 154-166.

Haurwitz, B. (1946) Insolation in Relation to Cloud Type. *J. Appl. Meteor.*, 3, 123-124.

Haurwitz, B. (1948) Insolation in Relation to Cloud Type. *J. Appl. Meteor.*, 5, 110-113.

Hay, J.E. (1970b) Precipitable Water Over Canada. *Atmosphere*, 8, 128-143.

Houghton, H.G. (1954) On the Heat Balance of the Northern Hemisphere. *J. Meteorol.*, 11, 1-9.

Idso, S.B. (1970) The Transmittance of the Atmosphere for Solar Radiation on Individual Clear Days. *J. Appl. Meteorol.*, 9, 239-241.

Kondratyev, K.Y. (1969) *Radiation in the Atmosphere*. Academic Press, New York.

Liou, K-N. (1976) On the Absorption, Reflection and Transmission of Solar Radiation in Cloudy Atmospheres. *J. Atmospheric Sci.*, 33, 798-805.

Monteith, J.L. (1962) Attenuation of Solar Radiation: A climatological study. *Quart. J. Roy. Meteorol. Soc.*, 88, 508-521.

Monteith, J.L. (1973) *Principles of Environmental Physics*, Edward Arnold Publishers Ltd., London.

Robinson, N. (1966) ed. *Solar Radiation*. Elsevier Publishing Co., New York.

Robinson, P.J. (1977) Measurements of Downward Scattered Solar Radiation From Isolated Cumulus Clouds. *J. Appl. Meteorol.*, 16, 620-625.

Wesely, M.L. and Lipschutz, R.C. (1976) A Method for Estimating Hourly Averages of Diffuse and Direct Solar Radiation Under a Layer of Scattered Clouds. *Solar Energy*, 18, 467-473.

APPENDIX 1

BUFFALO RADIOSONDE DATA AND PRECIPITABLE WATER CALCULATIONS

A. Buffalo Radiosonde Data: July 8, 1200Z

Pressure (kPa)	Temperature (°C)	Dewpoint Depression (°C)
surface 101.3	16.0	2.2
99.7	17.0	2.3
95.4	17.4	8.0
82.0	8.8	8.0
80.3	9.4	21.0
78.4	8.6	22.0
77.2	8.8	3.0
76.2	9.2	6.0
73.4	7.0	1.5
67.7	5.6	8.0
63.2	2.2	13.0
61.5	0.4	6.0
60.4	-1.3	0.1
57.1	-2.1	0.0
54.8	-3.9	2.1
54.0	-4.1	4.0
51.7	-6.9	2.9
50.0	-7.5	7.0
47.1	-11.7	3.9
42.1	-16.9	16.0
33.7	-25.7	30.0
27.0	-39.1	11.0

B. Buffalo Radiosonde Data: July 9, 1200Z

Pressure (kPa)	Temperature (°C)	Dewpoint Depression (°C)
surface 101.2	13.8	0.0
100.0	13.6	1.3
85.0	13.4	3.7
70.0	5.8	14.0
50.0	-7.5	30.0
40.0	-18.5	10.0
30.0	-32.5	13.0

C. Buffalo Radiosonde Data: July 13, 1200Z

Pressure (kPa)	Temperature (°C)	Dewpoint Depression (°C)
surface 99.3	15.6	0.5
94.7	13.0	0.0
92.8	16.0	0.0
90.7	16.6	0.0
78.5	10.6	0.0
74.6	8.4	2.7
66.7	2.6	0.0
66.4	0.6	30.0
65.1	3.4	20.0
55.9	-4.3	30.0
52.5	-7.3	3.1
50.0	-9.3	4.6
49.4	-9.7	30.0
47.5	-10.3	30.0
44.7	-13.5	7.0
41.8	-17.3	11.0
38.9	-22.5	4.2
32.9	-30.1	0.0
27.9	-39.3	4.7

D. Buffalo Radiosonde Data: August 18, 1200Z

Pressure (kPa)	Temperature (°C)	Dewpoint Depression (°C)
surface 97.9	12.2	5.0
92.3	8.2	3.8
86.5	5.0	6.0
85.0	5.2	9.0
76.6	1.2	19.0
70.0	-2.1	30.0
65.5	-4.1	18.0
63.2	-4.1	17.0
59.3	-6.3	17.0
50.0	-13.3	14.0
40.0	-25.9	13.0

E. Precipitable Water: July 8, 1200Z

Pressure (kPa)	Temperature (°C)	Specific Humidity ($\bar{q}_i$)	Precipitable Water (w_i)
101.3	16.0	.00969	1.5838
99.7	17.0	.01044	3.7331
95.4	17.4	.00769	7.5112
82.0	8.8	.00491	0.4842
80.3	9.4	.00195	0.2843
78.4	8.6	.00172	0.4406
77.2	8.8	.00743	0.5427
76.2	9.2	.00628	1.5143
73.4	7.0	.00766	2.6108
67.7	5.6	.00471	1.1538
63.2	2.2	.00264	0.3839
61.5	0.4	.00407	0.3524
60.4	-1.3	.00560	1.1886
57.1	-2.1	.00559	0.6955
54.8	-3.9	.00418	0.1869
54.0	-4.1	.00354	0.4573
51.7	-6.9	.00318	0.2603
50.0	-7.5	.00215	0.3388
47.1	-11.7	.00206	0.3217
42.1	-16.9	.00041	0.0856
33.7	-25.7	.00003	0.0158
27.0	-39.1	.00009	0.0189
16.4	-61.9	.00003	24.1645 = W

F. Precipitable Water: July 9, 1200Z

Pressure (kPa)	Temperature (°C)	Specific Humidity ($\bar{q}_i$)	Precipitable Water (w_i)
101.2	13.8	.00970	1.1039
100.0	13.6	.00890	12.2364
85.0	13.4	.00881	7.0236
70.0	5.8	.00293	2.0499
50.0	-7.5	.00021	0.2338
40.0	-18.5	.00068	0.1782
30.0	-32.5	.00014	22.8258 = W

G. Precipitable Water: July 13, 1200Z

Pressure (kPa)	Temperature (°C)	Specific Humidity ($\bar{q}_i$)	Precipitable Water (w_i)
99.3	15.6	.01076	4.5375
94.7	13.0	.00984	1.9471
92.8	16.0	.01220	2.4048
90.7	16.6	.01296	12.0274
78.5	10.6	.01013	2.7370
74.6	8.4	.00764	4.2584
66.7	2.6	.00687	0.0786
66.4	0.6	.00050	0.0956
65.1	3.4	.00159	0.5623
55.9	-4.3	.00026	0.3326
52.5	-7.3	.00297	0.3797
50.0	-9.3	.00227	0.0414
49.4	-9.7	.00016	0.0171
47.5	-10.3	.00016	0.1138
44.7	-13.5	.00136	0.1499
41.8	-17.3	.00067	0.1063
38.9	-22.5	.00085	0.2065
32.9	-30.1	.00070	0.0864
27.9	-39.3	.00018	30.0825 = W

H. Precipitable Water: August 18, 1200Z

Pressure (kPa)	Temperature (°C)	Specific Humidity ($\bar{q}_i$)	Precipitable Water (w_i)
100.0	11.6	.00645	1.3255
97.9	12.2	.00646	3.2119
92.3	8.2	.00564	2.5536
86.5	5.0	.00408	0.4871
85.0	5.0	.00332	1.5974
76.6	1.2	.00122	0.3812
70.0	-2.1	.00027	0.1743
65.5	-4.1	.00060	0.1370
63.2	-4.1	.00091	0.2212
59.3	-6.3	.00078	0.4001
50.0	-13.3	.00062	0.2234
40.0	-25.9	.00022	10.7128 = W

APPENDIX 2

CLOUD DATA

A. July 8

Time (GMT)	Total Cloud (tenths)	Cloud Amount (tenths) Mt. Hope	McMaster
1000	10	F10	
1037	10	F10	
1040	10	F10	
1055	10	F10	
1100	10	F6, ST4	
1115	10	F4, SF3, ST3	
1136	10	F4, SF4, ST2	
1200	10	F4, SF5, ST1	
1250	10	SF6, SC4	
1300	10	SF3, SC7	
1400	10	SF4, SC6	
1500	10	SF3, SC7	
1531	10	SC9, SC1	
1600	9	SC9	
1700	9	SC9	
1800	8	Cu8	Cu7
1900	7	Cu7	Cu8
2000	7	Cu7	Cu5
2100	5	Cu5	
2200	3	Cu2, Ci1	
2300	4	Cu2, Ci2	
0000	5	AC2, Ci2	

B. July 9

Time (GMT)	Total Cloud (tenths)	Cloud Amount (tenths) Mt. Hope	McMaster
1100	9	F1, AC8	
1148	9	SC1, AC8	
1200	9	SC3, AC6	
1300	10	SC9, AC1	
1400	7	SC3, AC4	Cu3
1500	5	AC5	
1600	3	Cu1, AC2	Cu1

Time (GMT)	Total Cloud (tenths)	Cloud Amount (tenths) Mt. Hope	McMaster
1700	3	Cu2, AC1	Cu2
1800	4	Cu4	Cu5
1900	4	Cu4	
2000	5	Cu5	
2100	6	TCu6	
2200	6	TCu6	
2300	6	Cu6	
0000	4	SC4	

C. July 13

Time (GMT)	Total Cloud (tenths)	Cloud Amount (tenths) Mt. Hope	McMaster
1000	3	F2, AC1	
1038	2	F2	
1100	2	F2	
1134	2	F2	
1200	1	Ci1	
1300	0		
1400	1	Cu1	Cu1
1500	2	Cu2	Cu1
1600	2	Cu2	Cu3
1700	4	Cu4	Cu6
1800	5	Cu5	Cu7
1900	6	Cu6	Cu8
2000	6	Cu6	
2100	6	Cu6	
2200	5	Cu5	
2300	4	Cu4, Ci1	
0000	2	Cu2	

D. August 18

Time (GMT)	Total Cloud (tenths)	Cloud Amount (tenths) Mt. Hope	McMaster
1000	1	CF1	
1100	1	Cu1	
1200	1	CF1	
1300	2	Cu2	
1400	6	Cu6	
1500	7	Cu7	
1600	6	Cu6	
1700	6	Cu6	

Time (GMT)	Total Cloud (tenths)	Cloud Amount (tenths)	
		Mt. Hope	McMaster
1800	6	Cu6	
1900	6	Cu6	
2000	5	Cu5	
2100	4	Cu4	
2200	3	Cu3	
2300	2	Cu2	
0000	2	Cu1, Ci1	